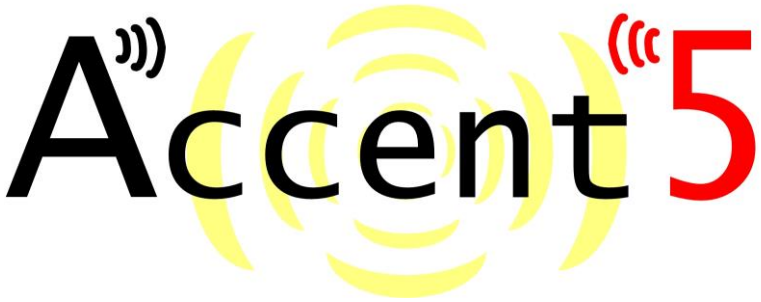

Project full title: Advanced Waveforms, MAC Design and Dynamic Radio Resource Allocation for Device to-Device in 5G Wireless Networks

Project acronym: **ACCENT5**
N° ANR-14-CE28-0026-01

Deliverable 1.2

"Advanced FB-MC for D2D communications"

Contractual date	T0+24
Actual date	13 January 2017
Version number	1.0

Lead Beneficiary	CentraleSupélec (CS)
Participants	Rostom Zakaria, Didier Le Ruyet (CNAM), Quentin Bodinier, Carlos F. Bader (CS).

Dissemination Level:	**Public**
Nature:	R
Total number of pages	39

Keywords list: D2D, Coexistence, PSD model, Interferences table, flexible waveforms, 5G, underlay communication.

Executive Summary

The focus of the ACCENT5 project is to study advanced techniques to enable the efficient introduction of device-to-device (D2D) communications in the next generation of cellular wireless networks (5G). In order to provide a clear overview of the context in which the project will evolve, this deliverable presents the main characteristics of potential multicarrier waveforms (at PHY layer) for D2D communications to be able to coexistence with deployed cellular users in the cell.
After defining and describing the different technical characteristics of the potential waveforms for 5G (FMT, FBMC, GFDM, and Lapped-FBMC) coexistence capabilities have been analysed and compared for two scenarios; that named homogeneous, where both cellular users and D2D devices use same PHY (i.e. CP-OFDM) layer, and second named, heterogeneous environment where the cellular users use the CP-OFDM (following the LTE standard) and D2D users use FBMC scheme.
A special attention is dedicated to modelling the interference and the bits transmitted in function of available OFDM time symbols in the transmission window.

A specific scheme named FFT-FBMC, has been also presented for the first time in this project to combat the FBMC intrinsic interference and enable some MIMO techniques such as Space-time Blokc Coding (STBC) and Maximum-Likelihood Spatial Multiplexing (ML-SM). Indeed, FFT-FBMC performs FFT/IFFT precoding and postcoding on each subcarrier in order to get rid of the FBMC intrinsic interference. A deep analysis on the robusteness of this last proposed PHY scheme is carried out in this deliverable, and also the impact of the asynchronism on the FFT-FBMC performances is studied .

In conclusion, this deliverable includes a deep analysis and a common reference on which the 5G candidate waveforms and their technical performances are compared and presented in order to have a coherent progress on the coexistence capabilities between cellular users and the D2D.

TABLE OF CONTENTS

LIST OF FIGURES

LIST OF TABLES

1 Introduction

This deliverable is the second technical document of task 1 of the ACCENT5 project, and it focuses on the use of advanced filter bank based multicarrier (FB-MC) schemes for D2D communications.
The deliverable is organised as followed: in Section 1, the structure and the characteristics of the candidate waveforms for 5G communication networks are presented.
In Section 3, a deep study is undertaken to analyse the effect of the time-frequency misalignment on the different 5G waveform. In this Section, we have analysed the coexistence aspects, and how to model the interference for two environments (homogeneous, and heterogeneous). A detailed analysis is presented on the suitability or not of the use of the PSD model for modelling the interference. Several numerical results are depicted with comparisons between interference values obtained with: (a) OFDM/OQAM onto CP-OFDM with PSD-based model, (b) OFDM/OQAM onto CP-OFDM through numerical simulation, and (c) CP-OFDM onto CP-OFDM with mean interference tables, and also the mean normalized EVM and the BER performances in homogeneous and heterogeneous scenarios. The main conclusions related to the use of D2D of the different 5G potential PHY layers are also underlined.
Section 4, is also an important part of this deliverable presenting a new multicarrier scheme (named FFT-FBMC). In this Section, the PSD analysis and achieved interference level are analysed using different time and frequency shifting, and two tables depicting the values of the interference power by averaging over the whole communication frame, and over one symbol duration are presented to show the FFT-FBMC potentialities for coexistence in D2D communication environment.

A general conclusion is presented in Section 5, on the main potential of each of the analysed waveforms and their suitability for D2D communications environments.

2 Analysed waveforms

We consider in our analysis, an OFDM based incumbent network with subcarrier spacing ΔF where a certain group of subcarriers is unused and can be utilized by a D2D pair. It is assumed that the base station provides information about its unused time-frequency resources. This information includes the number of free subcarriers M_f, the number of OFDM symbols during which the band will be free N_f. We define B_i as the band occupied by the primary users, B_f the free band used by the D2D pair, and I_{th} as the interference threshold for B_i. The D2D pair starts transmitting in the free band in an asynchronous fashion in time with respect to the primary users. Besides, it is assumed that the D2D pair can be also misplaced in frequency with respect to the incumbent network.

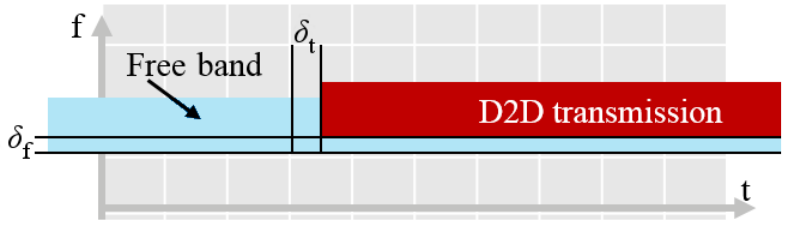

Figure 1: Time-Frequency layout of the situation with time-frequency misplacement representation.

We denote δ_t and δ_f as the offsets in time and frequency. The scenario is presented in Figure 1, where the grey grid represents the time-frequency resources of the incumbent network. These resources can follow the same trend as that of 3GPP Long Term Evolution (LTE) standard.
To pave the way for the analysis conducted in Section 3.2, we briefly explain the mathematical representation of the waveforms under study to be used by the D2D pair in the following:

OFDM/OQAM:
Recently, there has been a growing interest in orthogonal frequency division multiplexing offset QAM (named also filter bank multicarrier (FBMC)) as one of the potential enabling technologies for 5G wireless communications. Indeed, OFDM/OQAM is considered as one of the broadband multicarrier techniques that may address the shortcomings of OFDM while maintaining some of its advantages. In contrast to OFDM that is based on rectangular pulse shape, the concept of FBMC is that the modulated data at each subcarrier is shaped by a time-frequency well-localized prototype filter. The utilization of well-designed waveforms provides an efficient and flexible access to fragmented spectrum offering thus a substantial enhancement in spectrum efficiency. However, a multicarrier system cannot simultaneously employ well-localized waveforms, keep complex orthogonality, and transmit at the Nyquist rate. In order to breakthrough this bottleneck, it has been demonstrated that it is possible to achieve interference-free transmission at baud rate subcarrier spacing in a multichannel QAM system as follows:

- Choosing a symmetric root-Nyquist filter at the transmitter and using the same as a matched filter at the receiver.
- Introducing a half symbol period delay between the in-phase and quadrature components of the QAM symbols.

In this modulation format, the signal can be derived in a similar way to FMT (see hereafter), where $P = M$, $\{d_m\}$ symbols are drawn from a PAM constellation, and a phase factor $\theta_m[n] = e^{j\frac{\pi}{2}\lfloor\frac{n+m}{2}\rfloor}$ is introduced where n and m the time-frequency indexes respectively. Besides, subsequent symbols are separated by $M/2$ samples in time, which implies doubling the symbol rate. Therefore, the transmit signal can be expressed as [18]

$$x_{\mathrm{OQAM}}[k] = \sum_{n=0}^{N-1}\sum_{m=0}^{M-1}\left(d_m[n]\theta_m[n]g[k-n\frac{M}{2}] \times e^{j2\pi\frac{m}{M}(k-\frac{KM-1}{2})}\right), \quad \forall k = 0\ldots(N+K-\frac{1}{2})M-1. \tag{2-1}$$

GFDM:
Generalized frequency-division multiplexing (GFDM) is a recent PHY layer scheme proposed to overcome some of the major broadband challenges in future communication systems (5G). The basic idea lies in the transmission of block frames composed of M time slots with *K* subcarriers. In GFDM, the out of-band radiation of the transmit signal is controlled by an adjustable pulse shaping filter that is applied to the individual subcarriers. The filter impulse response *g* plays an important role in the system and it is not restricted to be rectangular as symbol pulse shapes like root-raised-cosine (RRC), Xia, or Gaussian can be used. The input bits are converted into *K* data streams that feed *K* independent mappers. Each mapper converts a block of bits into a data symbol to be transmitted and since they are independent, different constellations can be used for each steam allowing a dynamic mapping. Note that there might be inter-carrier interference (ICI) among adjacent subcarriers and inter-symbol interference (ISI) might arise if the transmit and receive filters do not fulfil the Nyquist criteria. Furthermore, GFDM applies (non-staggered) quadrature amplitude modulation (QAM), which results in non-orthogonal subcarriers, unless rectangular pulse shape is used. Therefore, an appropriate interference cancelling is needed at the receiver to match to the performance of OFDM.

The data is packed in blocks of N_b symbols and a CP is added to the beginning of each block. Every symbol is circularly convolved with a time shifted version of the same circular filter *g*. Noting mod the modulo operation, the signal corresponding to one GFDM block is expressed as follows [14]

$$x_{\mathrm{GFDM}}[k] = \sum_{n=0}^{N_\mathrm{b}-1} \sum_{m=0}^{M-1} d_m[n] g\left[(k-nM) \mathrm{mod}(N_\mathrm{b} M)\right] e^{j2\pi k \frac{m}{M}}, \quad \forall k = 0 \dots MN_\mathrm{b} - 1. \tag{2-2}$$

FMT:
On the contrary to OFDM scheme, filtered multi-tone modulation (FMT) exploits a form of poly-phase filter-bank modulation where a high level of spectral containment is achieved by sub-channel spectral shaping with non-overlapping sub-bands. In FMT, we do not need to use a prefix between symbols. Instead, the bandwidth of each of the sub-carriers is chosen to be quasi orthogonal in the frequency domain. This is achieved by the use of steep roll-off band-pass filters. The time domain response of these filters may overlap several successive transmitted symbol periods, but are close to being orthogonal in the frequency domain at both channel input and output. Thanks to this property, the FMT scheme uses QAM symbols to transmit information and, in contrast to FBMC schemes, avoids the need of using offset-QAM (OQAM) modulation to reach orthogonality. In this scheme, complex Quadrature Amplitude Modulation (QAM) symbols are linearly pulse shaped using the prototype filter $\mathbf{g} = [g[0] \dots g[KP-1]]^\mathrm{T}$, where *K* is the overlapping factor and *P* is the number of samples per time symbol. *M* is the number of subcarriers, *N* the number of symbols in time, and $\mathbf{d}_m = [d_m[0] \dots d_m[N-1]]^\mathrm{T}$ the vector of modulated symbols on the *m*th subcarrier. Finally, the FMT signal can be obtained as [9]

$$x_{\mathrm{FMT}}[k] = \sum_{n=0}^{N-1} \sum_{m=0}^{M-1} d_m[n] g[k-nP] e^{j2\pi \frac{m}{M} k}, \quad \forall k = 0 \dots (N+K-1)P - 1. \tag{2-3}$$

Lapped FBMC: This scheme is in essence similar to OFDM/OQAM systems. However, for this modulation the symbol rate is not doubled. The carriers are spaced by 1/2*M* instead of 1/*M* for OFDM and each of the 2*M* real data samples to be transmitted is allocated a sub-channel in the filter bank, this is pulse amplitude modulation (PAM) instead of QAM. Therefore, the approach can be named FBMC-PAM [12].
As defined in [12], the emitted signal can be written as

$$x_{\mathrm{Lapped}}[k] = \sum_{n=0}^{N-1} \sum_{m=0}^{M-1} d_m[n] g[k-nM] e^{j(k-\frac{1}{2}+\frac{M}{2})(m-\frac{1}{2})\frac{\pi}{M}}, \quad \forall k = 0 \dots (P+1)M - 1. \tag{2-4}$$

$$g_{\text{Lapped}}[k] = -\sin\left[(k-\frac{1}{2})\frac{\pi}{2M}\right], \forall k = 0 \dots 2M-1.$$

FFT-FBMC: Unlike the previously described waveforms, the FFT-FBMC, is a new scheme proposed in this project. Achieved performances of this last scheme are separately detailed in Section 4.

In Table 1, we provide the number of data symbols useful to D2D pairs. In order to make a fair comparison, we have taken into account the loss of the CP for the non OFDM waveforms.

Table 1: Number of data symbols useful to D2D pairs

Waveform	Useful D2D Symbols
OFDM	N_{f}
FMT	$N_{\text{f}} - K + 1$
OFDM/OQAM	$\lfloor N_{\text{f}}\frac{M+N_{\text{CP}}}{M} - K + \frac{1}{2}\rfloor$
Lapped FBMC	$\lfloor N_{\text{f}}\frac{M+N_{\text{CP}}}{M} - 1\rfloor$
GFDM	$N_b\lfloor\frac{N_{\text{f}}}{N_{\text{b}}}\frac{N_{\text{b}}(M+N_{\text{CP}})}{N_{\text{b}}M+N_{\text{CP}}}\rfloor$

3 Waveforms for overlay D2D communications

The advent of Device-To-Device (D2D) communication as a new application in 5th Generation of wireless networks (5G) raises a large number of challenges. In particular, coexistence of D2D pairs with primary users may affect the incumbent network. To avoid that, a first standard for D2D communication has been proposed [1], but it still requires consequent interaction between the base station and the D2D pairs. This, in turn, may impose a large amount of network overhead due to control signalling. In the scenario we study, the base station only informs the D2D pairs of the available time-frequency resources. This paradigm has two main challenges to overcome: (i) time and frequency alignment of the D2D signal cannot be assumed to be perfect with respect to the incumbent network. (ii) D2D users have to respect strict spectral requirements in order to limit interference to primary users. To the best of our knowledge, there is no study available in the literature looking into the effect of time-frequency misalignment from a given waveform onto Orthogonal Frequency Division Multiplexing (OFDM), i.e. challenge (i). The previous studies on time-frequency misalignment effects are bounded to the case where the misaligned user has the same waveform as the primary ones [2], [3]. To address challenge (ii), a large body of work is available in the literature that is based on power loading techniques and waveform design [4]–[14].

Power loading based solutions aim at solving optimization problems where D2D pairs try to maximize their rate subject to constraints such as total power budget and maximum interference that primary users can tolerate. Such problems have already been thoroughly studied in the literature and near optimal, low complexity solutions have been proposed [4]–[7].
The study of optimal resource allocation methods is therefore out of the scope of this paper. Instead, this paper provides the interference tables to be used in the optimal power loading solution of [6] for different waveforms. As a matter of fact, the rate achievable by D2D users is highly dependent on their air interface. Indeed, utilization of well localized waveforms can limit Out Of Band (OOB) emissions of D2D users and therefore allows them to allocate higher power to their active subcarriers. It is well known that OFDM suffers from large side lobes in frequency due to its rectangular window in time [11], [15], [16]. To overcome this problem, numerous solutions have been proposed [11]. Despite their variety, they all rely on filtering techniques that bring bandwidth efficiency loss. To avoid that, a number of new waveforms with intrinsic filtering properties have emerged. [7]–[14].

These waveforms all rely on Filter Bank Multi Carrier (FBMC), an idea that was raised 50 years ago [17] and is considered as a candidate for 5G systems. In this work, we focus on four recently proposed FBMC based waveforms, namely Filtered Multi-Tone (FMT), Offset Quadrature Amplitude Modulated-Orthogonal Frequency Division Multiplexing (OFDM/OQAM), Lapped FBMC and GFDM.

In FMT modulation [8][9], the assumption is that there is no overlapping between adjacent subcarriers. Therefore, FMT suffers from some bandwidth efficiency loss. To increase spectral efficiency, OFDM/OQAM [10], [11] allows for adjacent subcarriers to overlap. Opposed to FMT, real symbols having Pulse Amplitude Modulation (PAM) are transmitted on each subcarrier. A $\frac{\pi}{2}$ phase difference is applied to adjacent subcarriers, which provides real-domain orthogonality. However, OFDM/OQAM requires doubling the symbol rate. To avoid that, Lapped FBMC modulation has been recently proposed by Bellanger et al. in [12]. In this scheme, the number of subcarriers is doubled instead of the number of time symbols. A drawback common to all the aforementioned modulations is the transient imposed by their transmitter and receiver filters.
Generalized Frequency Division Multiplexing (GFDM) tackles this problem by application of cyclic pulse shaping [13]. However, this comes at the expense of higher OOB emissions, which is due do the discontinuities induced in the signal by truncation in time with a rectangular window [14].

We analyse in this documents the time-frequency misalignment effects of the D2D pair on the incumbent network. We evaluate the interference injected from D2D pair to the incumbent network for each waveform separately. This allows us to build interference tables to be used as inputs to the power loading solution and analyse the maximum rate achievable through each waveform. We consider different resource sizes in time and frequency and calculate the maximum amount of information that can be transmitted. This analysis reveals the strength and weaknesses of different waveforms to be used by the D2D pair as a function of available time-frequency resources.

3.1 Effect of the time-frequency misalignment

To assign the optimal power distribution to the D2D subcarriers, it is vital to know how much power leaks to the adjacent band depending on which waveform is utilized by the D2D pair. The classical way to compute the leakage is to integrate the Power Spectral Density (PSD) of the interfering signal on the band that suffers from the interference. However, this model does not take into account the time window of the incumbent. This is of paramount importance as the incumbent only considers a time window with a specific width based on its own parameters. Besides, it has been shown in [19] that PSD is not a suitable measure to evaluate the intersystem interference for the scenario of interest to this document.
We therefore employ the instantaneous interference model proposed in [19] to compute the interference I^l_m injected to the l-th subcarrier of the incumbent by the D2D signal x_m where only subcarrier m is utilized. This allows us to scrutinize the interference injected by each individual subcarrier to the incumbent network. Note that the same subcarrier spacing is used for both the D2D pair and the incumbent network.

3.2 Interference analysis

To assign the optimal power distribution to the D2D subcarriers, it is vital to know how much power leaks to the adjacent band depending on which waveform is utilized by the D2D pair. The classical way to compute the leakage is to integrate the Power Spectral Density (PSD) of the interfering signal on the band that suffers from the interference. However, this model does not take into account the time window of the incumbent. This is of paramount importance as the incumbent only considers a time window with a specific width based on its own parameters. Besides, it has been shown in [19] that PSD is not a suitable measure to evaluate the intersystem interference for the scenario of interest to this deliverable.

We therefore employ the instantaneous interference model proposed in [19] to compute the interference I^l_m injected to the lth subcarrier of the incumbent by the D2D signal x_m where only subcarrier m is utilized. This allows us to scrutinize the interference injected by each individual subcarrier to the incumbent network. Note that the same subcarrier spacing is used for both the D2D pair and the incumbent network. Therefore, we have

$$I^l_m = \int_{t=0}^{T} \left| \left(g^l_r * x_m\right)(t) \right|^2 dt, \tag{3-1}$$

where g^l_r is the receiver filter on subcarrier l and ($*$) denotes the convolution operation. As the receiver suffering from interference is based on OFDM, becomes

$$I_m^l = \sum_{n=0}^{N-1} \frac{T_\mathrm{s}}{M+N_\mathrm{CP}} \sum_{k=n(M+N_\mathrm{CP})+N_\mathrm{CP}}^{(n+1)(M+N_\mathrm{CP})} \left| x_m[k] e^{-j2\pi k \frac{l}{M}} \right|^2, \tag{3-2}$$

where N is the total number of OFDM symbols corresponding to the time span T, N_{CP} is the number of CP samples and M the number of samples per OFDM symbol of length T_s. Therefore, by taking into account timing and frequency offsets between the interferer and the receiver, we have

$$I_m^l(\delta_\mathrm{t}, \delta_\mathrm{f}) = \sum_{n=0}^{N-1} \left(\frac{T_\mathrm{s}}{M+N_\mathrm{CP}} \sum_{k=n(M+N_\mathrm{CP})+N_\mathrm{CP}}^{(n+1)(M+N_\mathrm{CP})} \left| a_m[k] e^{j2\pi \left(k \frac{m-l+\delta_\mathrm{f}}{M} + \frac{\delta_\mathrm{t}}{M} \right)} \right|^2 \right). \tag{3-3}$$

Then, the mean interference seen at subcarrier l at the receiver of the incumbent can be written as

$$I_{m_\mathrm{mean}}^l(\delta_t, \delta_f) = \frac{1}{N} E_{d_m}(I_m^l(\delta_t, \delta_f)), \tag{3-4}$$

where E_{dm} represents the expectation with respect to the symbols transmitted on subcarrier m. We point out that when a larger number of subcarriers are utilized by the D2D pair, the total interference is equal to the sum of the interference caused by each subcarrier. Finally, the total interference injected by the D2D transmission on the free band B_f to the incumbent band B_i is

$$I_{B_\mathrm{i}}^{B_\mathrm{f}} = \sum_{m \in B_\mathrm{f},\ l \in B_\mathrm{i}} \frac{P_m}{P_0} I_{m_\mathrm{mean}}^l(\delta_\mathrm{t}, \delta_\mathrm{f}), \tag{3-5}$$

where P_m is the power assigned to the m-th subcarrier and P0 is a reference value of 1W. This method can be used to compute the interference tables for the different analysed waveforms.

3.2.1 Considering Transmission Window Duration

As a static interference constraint is assumed during the whole D2D transmission, we can simply compute the total number of bits transmitted as

$$b = T_\mathrm{useful} * \sum_{m=0}^{M_\mathrm{f}-1} \log_2(1 + \frac{P_m^*}{\sigma_\mathrm{N+I}^2}), \tag{3-6}$$

where T_{useful} is the duration in which useful symbols can transmitted. This value depends on the utilized waveform. Indeed, for filter banks with linear pulse shaping like FMT and Lapped FBMC, the overlapping factor K introduces a delay of $K - 1$ symbols in the time domain. For OFDM/OQAM, the delay imposed by transmitter and receiver filters is $K – 1/2$ symbols in time as symbols are separated by $T_s/2$. In contrast, OFDM and GFDM do not suffer from any delay. In fact, the block structure of GFDM brings some limitations as the length of the whole block is fixed for any number of active symbols. Thus, the transmission window can only be fully utilized in time if its duration is multiple of the GFDM block length.

We consider an incumbent system following similar parameters to 3GPP LTE standard. The OFDM primary user occupies 180 subcarriers, which corresponds to 15 LTE resource blocks along the frequency axis. Besides, it uses M = 180 samples per symbol and N_{CP} = 12 samples. The length of the transmission window in time varies from N_f = 1 to 100 OFDM symbols. In the centre of the incumbent band, a free band B_f divided into M_f subcarriers is unused. This band is utilized by the D2D pair. No guard band is considered in this study. The

parameters of each waveform under study for utilization by the D2D pair are listed in Table 2. RRC refers to the Root Raised Cosine filter.

Table 2: Proposed D2D Waveform Parameters

Waveform	Samples per symbol	CP samples	Filter	Overlapping factor.
OFDM	M	N_{CP}	Irrelevant	Irrelevant
FMT	$M + N_{CP}$	0	RRC, roll-off 0.2	6
OFDM/ OQAM	M	0	Phydias [18]	4
Lapped FBMC	M	0	Sine [12]	2
GFDM	M	N_{CP}	RRC, roll-off 0.2	5

We compute the interference caused by the D2D transmission according to the interference injected by one active subcarrier on the incumbent band as a function of δ_t *(time offset)* where $\delta_f = 0$ (*frequency offset*). We notice that OFDM based D2D transmission does not interfere at all if the timing offset is contained within the CP. However, when δ_t falls outside the CP, there is a big jump in the amount of interference to the incumbent band. On the other hand, the interference caused by other waveforms does not have a high variation with respect to δ_t. This result reveals that it may not be worth synchronizing D2D transmission in time with the primary users when different waveforms are utilized by the D2D pair.

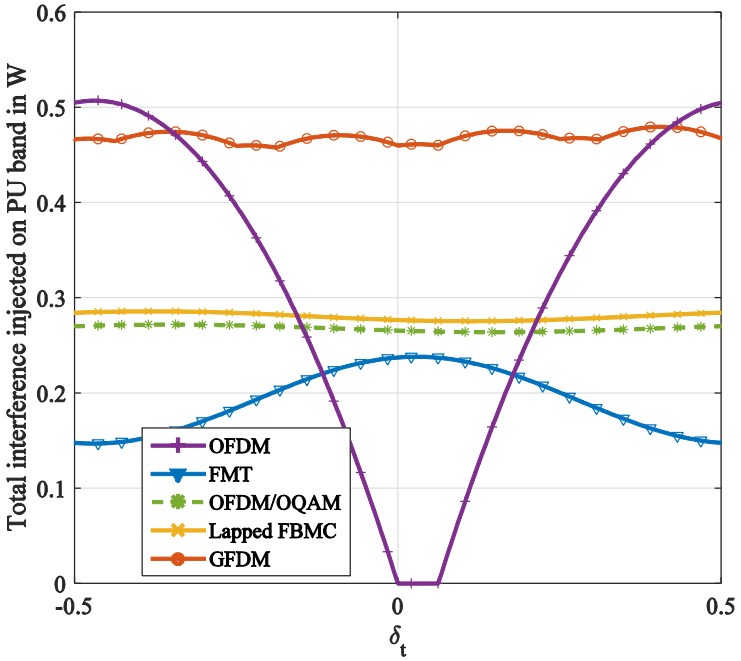

Figure 2: Total injected interference on the incumbent band as a function of δ_t. Timing offset has limited impact on injected interference except in the case where D2D transmitters use OFDM.

Computation of Interference Tables

In addition, we evaluate the interference that is caused by the different waveforms. We present the mean and maximum interference tables with respect to δt in Figure 3a and 3b.

Our observations are threefold: First, it appears that OFDM is the only waveform that shows a significant difference between its mean and maximum injected interference on the OFDM based incumbent. Other waveforms show a difference of approximately 0 to 1dB. Second, if mean interference is considered, GFDM causes the highest interference. However, if the maximum interference is considered, OFDM based D2D pair has the worst performance. Third, we point out that values of interference injected by 5G waveforms are surprisingly high. For OFDM/OQAM for example, the PSD based model predicts an attenuation of -60 dB at subcarrier distance of 2 [19], whereas our interference tables show that the interference power seen by an OFDM receiver at subcarrier distance of 2 is -18.5 dB. This is due to the fact that the OFDM demodulator performs Fast Fourier Transform (FFT) on a time window that may be much shorter than the length of the

symbol of the other waveform. Therefore, the signal suffers from discontinuities that produce projections on the whole incumbent spectrum.

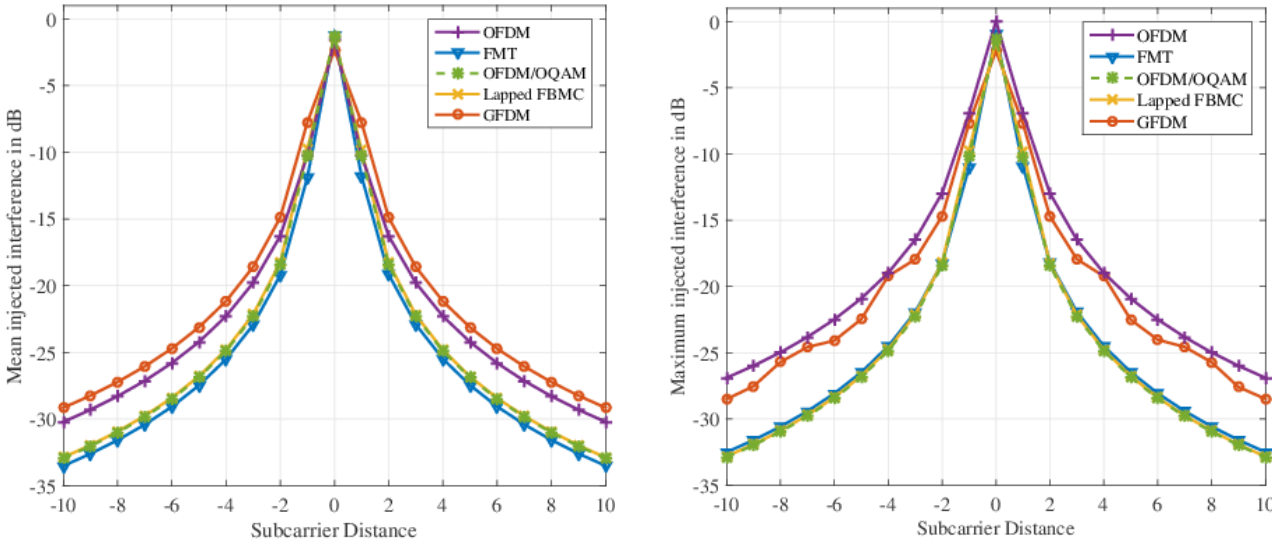

(a) Mean Interference Table on OFDM receiver

(b) Maximum Interference Table on OFDM receiver

Figure 3: Maximum and Mean interference tables seen by a subcarrier of OFDM receiver in function of its distance an active 5G waveform subcarrier

Finally, we point out that interference tables are presented for $\delta_f = 0$. However, as δ_f only acts as a frequency shift, when $\delta_f = 0$, the interference can be directly taken from interference tables by taking the corresponding subcarrier distance into account. As a case in point, if the subcarrier distance is -2 and $\delta_f = 1$, interference value corresponding to an actual subcarrier distance of -1 should be read from the table.

Transmission Performance

In this subsection, we consider the total amount of data that can be transmitted by the D2D pair during the transmission window as a measure to evaluate the performance of different waveforms. We use the interference tables derived in the previous subsection to calculate the total amount of data that can be transmitted during the transmission window based on the waveform that is utilised. We consider a transmission band consisting $M_f = 12$ free subcarriers, an interference constraint Ith of either 1W or 1 mW and variable number of time symbols $N_f \in [1, 100]$. Besides, the maximum frequency misalignment is one subcarrier spacing (i.e. $\delta_{fmax} = 1$).
The amount of data transmitted by the D2D pair as a function of N_f is obtained for two values of Ith in Figure 4. The presented results bring insight into which waveform to be used for different time window lengths and interference constraint. It seems that for transmission windows shorter than 10 symbols, OFDM is the best choice, as it does not suffer from any transmission delay. Therefore, linearly pulse shaped waveforms can compete only when the transmission window starts getting wider than 10 OFDM symbols. It can be noticed that Lapped FBMC shows a promising performance. This is due to the fact that it has a very short delay about only one symbol, and injects interference comparable to that of OFDM/OQAM and FMT. FMT suffers from a large amount of delay during transmission and seems not to be an appropriate candidate for such low latency application. However, OFDM/OQAM performance stays very close to the Lapped FBMC.

Interestingly, performance of OFDM starts to degrade for the time windows of width larger than $N_f = 15$ regardless of the interference constraint. This is the result of its spectral efficiency loss due to the presence of CP. Note that even though GFDM seems to be a potential competitor to OFDM/OQAM and Lapped FBMC when the interference constraint is very relaxed, it cannot efficiently cope with stringent interference constraints. This is the consequence of its high interference leakage as shown in Figure 3.

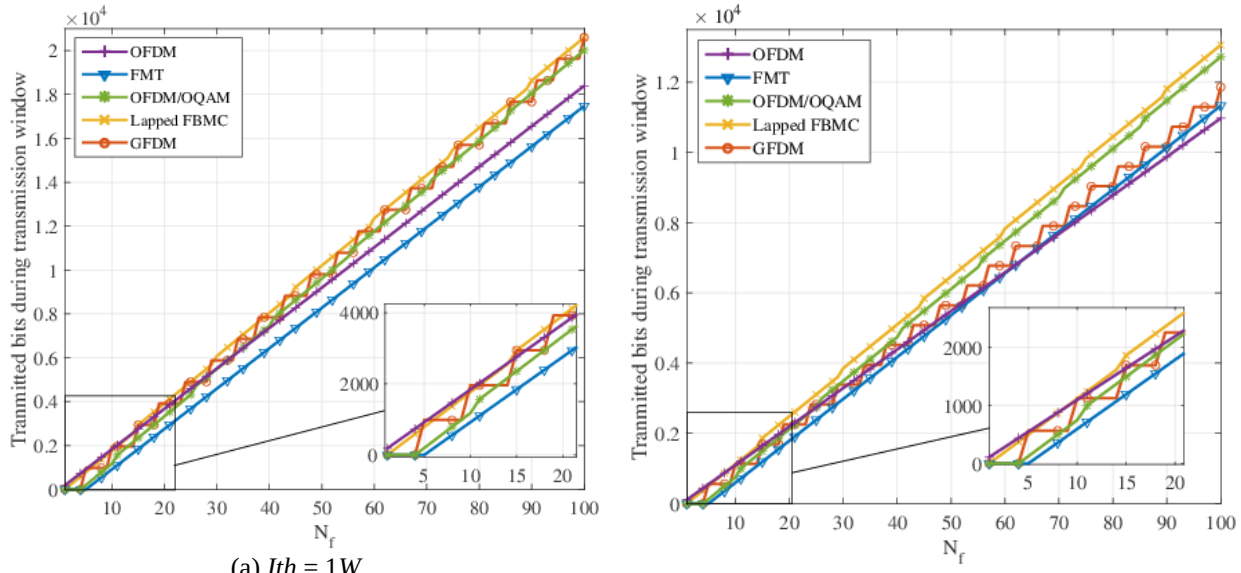

(a) *Ith* = 1*W* (b) *Ith* = 1*mW*

Figure 4: Bits transmitted in function of available OFDM time symbols in the transmission window

3.3 Modelling interference between OFDM/OQAM and CP-OFDM:

3.3.1 Modelling interference in heterogeneous environment

OFDM with Offset Quadrature Amplitude Modulation (OFDM/OQAM) [23], is one of the main new waveform schemes explored by the research community. Indeed, it overcomes the cited CP-OFDM limitations and enables both higher flexibility and reduction of interference leakage for multi-standard systems coexistence [11] [15] [16]. The coexistence between OFDM/OQAM based D2D pairs and CP-OFDM LTE users has been widely studied in [24]. In all studies on coexistence between OFDM/OQAM secondary users [25] [27] and CP-OFDM incumbent ones, the interference caused by the different types of users onto each other is quantified with the Power Spectral Density (PSD)-based model originally proposed in [29]. Yet, the authors pointed out in [27] that values of interference obtained by means of Monte-Carlo simulations were much higher than those obtained with the PSD-based model. In [30] Medjahdi *et. al.* designed a more precise interference model named ”instantaneous interference” that takes into account the demodulation operations and the time asynchronism between users. Nevertheless, the aforementioned study only analysed the multiuser interference in cases where all users are using the same waveform, either CP-OFDM or OFDM/OQAM. No such analysis has been applied to heterogeneous scenarios where CP-OFDM and OFDM/OQAM system are deployed in the same geographical area and coexist in the same cell.

Our approach in this section is therefore to study inter-user interference in scenarios where CP-OFDM and OFDM/OQAM users interfere with each other. It is shown that the PSD based approach consists in modelling the interference at the input antenna of the interfered receiver, and totally omits the demodulation operations that are performed by the latter. We show that the actual interference seen at the output of the demodulator of the interfered receiver is much higher than expected using the PSD based model. Moreover, we show that interference between the incumbent and secondary systems is symmetrical, which contradicts the results obtained with the PSD-based model. Finally, the presented study nuances the results classically shown in the literature, and diminishes the benefits expected from using OFDM/OQAM for coexistence with CP-OFDM incumbent systems.

3.3.2 Discussing the suitability of the PSD-based model

We consider for our analysis a simple scenario where an incumbent system $\mathcal{U}_1$ coexists with a secondary user $\mathcal{U}_2$ in the same band. Both systems use multicarrier waveforms with the same subcarrier spacing ΔF, and each of them is assigned a set of subcarriers L_i. The incumbent $\mathcal{U}_1$ utilizes CP-OFDM, whereas two alternatives are

studied for $\mathcal{U}_2$. The latter uses CP-OFDM in the case of a homogeneous scenario (referred to as *Hom*) and OFDM/OQAM in the case of a heterogeneous scenario (referred to as *Het*). The configurations studied in this paper are summarized in Figure 5. To focus the study on interference coming from the coexistence between these two systems, all channels are assumed perfect, and no Gaussian noise is considered. Considering an infinite transmission on M subcarriers, the sequences of symbols estimated at the receiver of $\mathcal{U}_1$ and $\mathcal{U}_2$ are modelled by

$$\begin{aligned} \hat{\mathbf{d}}_{1,m}[n] &= \mathbf{d}_{1,m}[n] + \boldsymbol{\eta}_m^{2\to1}[n], \\ \hat{\mathbf{d}}_{2,m}[n] &= \mathbf{d}_{2,m}[n] + \boldsymbol{\eta}_m^{1\to2}[n], \\ & \forall n \in N,\ \forall m = 0 \dots M-1 \end{aligned} \tag{3-7}$$

where $\mathbf{d}_{i,m}[n]$ is the n-th symbol transmitted on the m-th subcarrier by user $\mathcal{U}_i$, and $\boldsymbol{\eta}_m^{j\to i}[n]$ represents the interference injected by the user $\mathcal{U}_j$ onto the *n-th* time slot and *m-th* subcarrier of user $\mathcal{U}_i$.

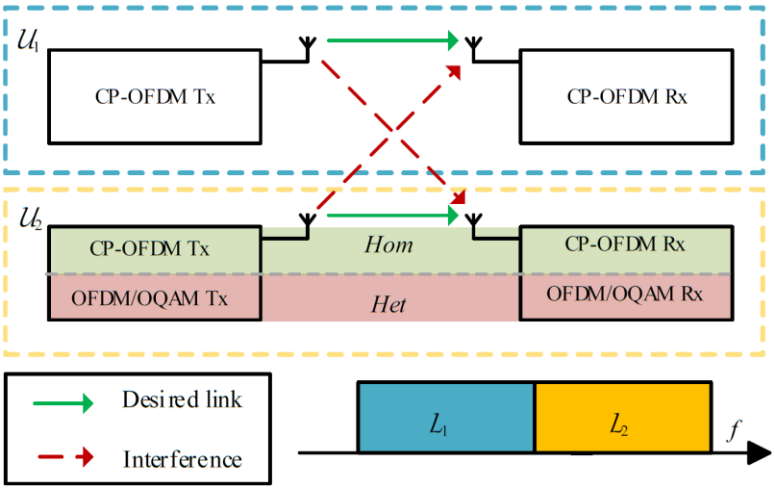

Figure 5: Summary of the study led in this Section: two users $\mathcal{U}_1$ and $\mathcal{U}_2$ transmit on adjacent bands L_1 and L_2 and interfere with each other. Channel is assumed perfect and no Gaussian noise is considered. $\mathcal{U}_2$ uses CP-OFDM in *Hom* scenario and OFDM/OQAM in *Het* scenario.

In both analysed scenarios, incumbent $\mathcal{U}_1$ and secondary $\mathcal{U}_2$ experience a loss of synchronization in time domain. Besides, the time duration between two subsequent CP-OFDM symbols transmitted by the incumbent system $\mathcal{U}_1$ is T_s+T_{CP}, where T_s is the time-symbol and T_{CP} accounts for the duration of the CP. It is assumed that the transmission of $\mathcal{U}_2$ starts with a delay τ with respect to the transmission of $\mathcal{U}_1$. The value of τ is taken as a random variable uniformly distributed in the interval $\left[-\frac{T_s+T_{CP}}{2}\ \frac{T_s+T_{CP}}{2}\right[$. Therefore, the interference injected by the users onto each other is a function of the symbols they transmit and of the value of τ. The mean interference power seen by each user on their m-*th* subcarrier is expressed as

$$\begin{aligned} I_m^{1\to2} &= E_{\mathbf{d}_1,\tau}\{|\boldsymbol{\eta}_m^{1\to2}[n]|^2\}, \\ I_m^{2\to1} &= E_{\mathbf{d}_2,\tau}\{|\boldsymbol{\eta}_m^{2\to1}[n]|^2\}, \end{aligned} \tag{3-8}$$

and the total interference injected by each user onto the other is

$$\begin{aligned} I^{1\to2} &= \sum_{m\in\mathcal{L}_2} I_m^{1\to2} \\ I^{2\to1} &= \sum_{m\in\mathcal{L}_1} I_m^{2\to1} \end{aligned} \tag{3-9}$$

The main pitfall of the PSD-based model lies in the fact that it does not take into account the time window of the receiver. However, this is of paramount importance as the incumbent only considers a time window with a specific width based on its own parameters. Though the PHYDYAS filter is well spectrally localized, it has a length of $L_{PHYDYAS} = KM$ samples. However, the CP-OFDM receiver window is of length $L_{CP\text{-}OFDM} = M$

samples. Therefore, the CP-OFDM incumbent demodulator performs Fast Fourier Transform (FFT) on a time window which is much shorter than the length of the prototype filter of OFDM/OQAM. In turn, the signal suffers from discontinuities that produce projections on the whole incumbent spectrum.
Moreover, the PSD based model consists in multiplying the interfering signal by a rectangular window in the frequency domain. In the time domain, this corresponds to filtering the interfering signal through an infinite sinc filter. Therefore, the PSD-based model does not reflect the actual demodulation operations that are processed at the CP-OFDM receiver that suffers from interference.

We consider a CP-OFDM system composed of M subcarriers out of which M_a are active. We define M vectors d_m such that d_m is constituted of complex Quadrature Amplitude Modulation (QAM) symbols if subcarrier m is active. Else, $d_m[n] = 0$, $\forall n \in \mathbb{N}$. N_{CP} being the length of the CP, the n-th OFDM symbol is expressed as

$$\begin{aligned} \mathbf{x}_n[k] &= \sum_{m=0}^{M-1} \mathbf{d}_m[n] e^{j2\pi \frac{m}{M} k}, \\ & n(M+N_{CP}) - N_{CP} \leq k \leq n(M+N_{CP}) + M - 1, \end{aligned} \tag{3-10}$$

To highlight the effects of inter-user interference only, we consider that the channel is perfect and that the CP-OFDM signal is polluted by an additive interfering signal y. In that case, the n-th CP-OFDM estimated symbol is

$$\begin{aligned} \hat{\mathbf{d}}_m[n] &= \mathbf{d}_m[n] + \underbrace{\sum_{k=n(M+N_{CP})}^{n(M+N_{CP})+M-1} \mathbf{y}[k] e^{j2\pi \frac{k}{M} m}}_{\boldsymbol{\eta}_m[n]}, \\ & 0 \leq m \leq M-1 \end{aligned} \tag{3-11}$$

where $\boldsymbol{\eta}_m[n]$ represent the total amount of interference that affects the estimated signal $\hat{\mathbf{d}}_m[n]$. The OFDM/OQAM system is composed of M subcarriers out of which M_a are active, where M vectors $\mathbf{d}_m$ contain real Pulse Amplitude Modulation (PAM) symbols if subcarrier m is active and $\mathrm{d}_m[n] = 0$, $\forall$n ∈ N otherwise. A phase factor $\theta_n[m] = e^{j\frac{\pi}{2}\lfloor \frac{n+m}{2} \rfloor}$ is further added to the symbols $\mathbf{d}_m[n]$. OFDM/OQAM is a based on a uniform polyphase filter bank structure with a prototype filter g of length $Lg = KM$, where K is called the overlapping factor, which is shifted to cover the whole of the system bandwidth. Subsequent symbols are separated by $M/2$ samples and are filtered through time frequency shifted versions of g. Therefore, each subcarrier is filtered by a filter $\mathbf{f}_m$ defined as:

$$\mathbf{f}_m[k] = \mathbf{g}[k] e^{j2\pi \frac{m}{M}(k - \frac{KM-1}{2})}, 0 \leq k \leq KM-1 \tag{3-12}$$

and the n-th modulated OFDM/OQAM symbol is written as

$$\begin{aligned} \mathbf{x}_n[k] &= \sum_{m=0}^{M-1} \mathbf{d}_n[m] \theta_n[m] \mathbf{g}[k - n\frac{M}{2}] \times e^{j2\pi \frac{m}{M}(k - \frac{KM-1}{2})}, \\ & (n-K)\frac{M}{2} \leq k \leq (n+K)\frac{M}{2} - 1 \end{aligned} \tag{3-13}$$

g is taken as the PHYDYAS filter with an overlapping factor $K = 4$ (details of the frequency response of **g** are available in [23]). At the receiver, each subcarrier is filtered through the matched filter $\tilde{\mathbf{f}}_m$ and the real part of the signal is taken to remove purely imaginary intrinsic interference [31] generated by the prototype filter **g**.

3.3.2.1 The mean interference

The amount of interference suffered by $\mathcal{U}_1$ and $\mathcal{U}_2$ on each of their subcarriers can be estimated from (3.10). In the *Hom* scenario, both $I^{1\to2}$ and $I^{2\to1}$ are obtained by replacing (3.9) in (3.10) respectively. These derivations lead to the following expressions of the interference caused by $\mathcal{U}_1$ (resp. $\mathcal{U}_2$) onto $\mathcal{U}_2$ (resp. $\mathcal{U}_1$):

$$\begin{aligned} I_{Hom}^{1\to2} &= \sigma_{\mathbf{d}_1^2} \sum_{m\in\mathcal{L}_2, q\in\mathcal{L}_1} I_{Hom}^{1\to2}(q-m), \\ I_{Hom}^{2\to1} &= \sigma_{\mathbf{d}_2^2} \sum_{m\in\mathcal{L}_1, q\in\mathcal{L}_2} I_{Hom}^{2\to1}(q-m), \end{aligned} \tag{3-14}$$

where $\sigma_{\mathbf{d}_i^2}$ is the variance of di. Besides, $\forall\ I_{Hom}^{1\to2}(l)$ (resp. $I_{Hom}^{2\to1}(l)$) represents the interference injected by the signal on the *q*-th subcarrier of $\mathcal{U}_1$ (resp. $\mathcal{U}_2$) onto the *m*-th subcarrier m of (resp. $\mathcal{U}_1$) where $l = q - m$ is called the spectral distance.
In *Hom* scenario, $\forall\ l$, $I^{1\to2}$ *Hom* (*l*) = $I^{2\to1}$ *Hom* (*l*), Mejdahdi *et. al.* have derived in [30] a closed-form of the interference I1→2 *Hom* (l) and tabulated its values in so-called "Mean Interference Tables". In *Het* scenario, the expression of $I^{1\to2}$ and $I^{2\to1}$ are obtained after some derivative, and have the following expressions:

$$\begin{aligned} I_{Het}^{1\to2} &= \sigma_{\mathbf{d}_1^2} \sum_{m\in\mathcal{L}_2, q\in\mathcal{L}_1} I_{Het}^{1\to2}(q-m), \\ I_{Het}^{2\to1} &= \sigma_{\mathbf{d}_2^2} \sum_{m\in\mathcal{L}_1, q\in\mathcal{L}_2} I_{Het}^{2\to1}(q-m). \end{aligned} \tag{3-15}$$

3.3.2.2 PSD-based Interference Modelling

The PSD-based model consists in computing the leakage caused by users onto each other by integrating the PSD of the interfering signal on the band that suffers from the interference. Therefore, in the *Het* scenario, according to the PSD-based model is obtained by computing

$$\begin{aligned} I_{Het}^{1\to2}(l) &= \int_{l-1/2\Delta F}^{l+1/2\Delta F} \Phi_{\text{CP-OFDM}}(f)df, \\ I_{Het}^{2\to1}(l) &= \int_{l-1/2\Delta F}^{l+1/2\Delta F} \Phi_{\text{PHYDIAS}}(f)df, \end{aligned} \tag{3-16}$$

where $\Phi_{\text{CP-OFDM}}$ (resp. Φ_{PHYDIAS}) is the PSD of the CP-OFDM signal (resp. of OFDM/OQAM with PHYDIAS filter). Because the PSD-based model only rates the power of injected interference, it is challenging to map the obtained values of interference to higher level metrics, e.g. Bit Error Rate (BER). The only possibility offered by the PSD-based model is to approximate the statistics of heterogeneous interference as a white Gaussian noise the variance of which is given by

$$\boldsymbol{\eta}_m^{2\to1} \sim \mathcal{N}(0, \sum_{q\in\mathcal{L}_\infty} I_{Het}^{2\to1}(q-m)). \tag{3-17}$$

Then, classical expressions of transmission performance under white Gaussian noise in [31] can be applied.

3.4 Numerical results

We consider an incumbent system $\mathcal{U}_1$ with 3GPP LTE standard parameters with M_a = 36 active subcarriers, which corresponds to 3 LTE resource blocks along the frequency axis, M = 256 samples per symbol and N_{CP} = 18 CP samples.

The secondary user $\mathcal{U}_2$ also uses 3 LTE resource blocks along the frequency axis. No guard band is considered between the two users, and they are directly adjacent in the spectrum. More specifically, the sets of subcarriers occupied by the two users are defined as $\mathcal{L}_1$ = [37 . . . 72] and $\mathcal{L}_2$ = [73 . . . 108]. Both users use the same subcarrier spacing ΔF = 15 kHz. In *Hom* scenario, CP-OFDM based $\mathcal{U}_2$ uses the same parameters as $\mathcal{U}_1$. In the *Het* scenario, OFDM/OQAM based $\mathcal{U}_2$ uses M = 256 samples per symbol and the PHYDIAS filter with overlapping factor K = 4. In *Het* scenario, the performance of users is evaluated though empirical estimation of (5) and (6) based on Monte-Carlo simulation and compared with the values expected with the PSD-based model. CP-OFDM systems transmit complex symbols drawn from a 64-Quadrature Amplitude Modulation (QAM) constellation. To ensure fairness, OFDM/OQAM systems transmit twice as much real symbols drawn from 8-Pulse Amplitude Modulation (PAM), which corresponds to a 64 QAM after reconstruction of a complex constellation. Moreover, $\mathcal{U}_2$ starts transmitting with a delay $\tau \in [-\frac{M+N_{\mathrm{CP}}}{2}\ \frac{M+N_{\mathrm{CP}}}{2}[$. Finally, numerical simulations are led on 105 symbols, each carrying 6 bits. Therefore, the BER curves drawn from numerical simulation are based on a transmission of 6 ×M_a × 105 = 1.92 × 107 bits.

First, we aim to rate the interference caused by $\mathcal{U}_2$ on the incumbent $\mathcal{U}_1$. Figure 6 presents the values of $I^{2\to1}(l)$ in dB for spectral distance $l \in [-20\ 20]$. For the *Het* scenario, i.e. when $\mathcal{U}_2$ uses OFDM/OQAM, we present values obtained with both the PSD-based model and through numerical simulations. We can observe in Figure 6 large gap between the values of interference planned by the PSD-based model and the real ones. As a case in point, at l = 2, the PSD-based model plans that the value of the interference injected on the incumbent will be about −65 dB, whereas numerical simulations show that the actual interference value is −18.5 dB.

Moreover, for l = 20, the PSD-based model predicts that the injected interference will be insignificant, whereas the numerical simulations show that it is still at a non-negligible level of −40 dB. This proves that in the *Het* scenario, the PSD-based model completely fails to give a good approximation of the interference injected by an OFDM/OQAM secondary user onto an incumbent CP-OFDM system.

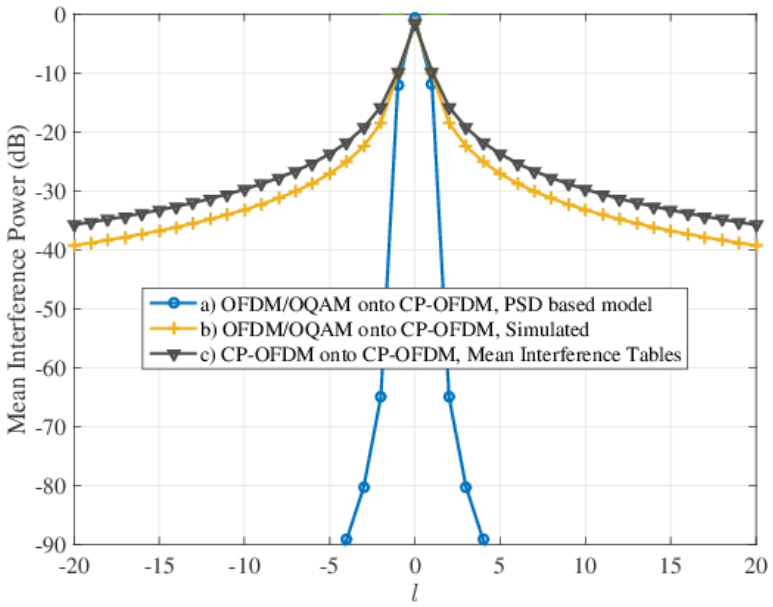

Figure 6: Comparison between interference values obtained with (a) OFDM/OQAM onto CP-OFDM with PSD-based model, (b) OFDM/OQAM onto CP-OFDM through numerical simulation, and (c) CP-OFDM onto CP-OFDM with mean interference tables [30][29].

We now focus on the transmission performance of both users. To do so, we set the power of the symbols transmitted by the incumbent system $\mathcal{U}_1$ as $\sigma^2_{d_2}$ = 0 dB and we sweep $\sigma^2_{d_2}$ from −20 dB to 20 dB. Here, we focus on the effects of inter-user interference caused by the adjacent transmissions of the two users. Therefore, no channel and no noise is considered. The normalized Error Vector Magnitude (EVM) obtained for both users is plotted in Figure 7. Here, our observations are threefold: first, the PSD-based model approximates surprisingly well the interference seen by the secondary OFDM/OQAM user $\mathcal{U}_2$ in the *Het* scenario. This shows that the PSD-based model may still be suitable in some cases, especially when the time window of the receiver is longer than the interfering signal. However, the PSD-based model dramatically underestimates the interference seen by the incumbent receiver $\mathcal{U}_1$. Second, we point out that the actual inter-user interference in the *Het*

scenario is symmetrical. As a case in point, the obtained EVM values for both users are equal when their transmission power is equal. This contradicts the PSD-based model, which predicts that the incumbent CP-OFDM $\mathcal{U}_1$ will be more protected than the secondary OFDM/OQAM $\mathcal{U}_2$: according to the PSD-based model, the normalized EVM values of both users are equal when $\sigma^2_{d_2} = 3$ dB. Third, both $\mathcal{U}_1$ and $\mathcal{U}_2$ experience lower EVM in the *Het* scenario than in the *Hom* scenario.

Note that the interfering signal is approximated to a white Gaussian noise to compute the BER from the EVM for both the PSD-based model in the *Het* scenario and the instantaneous interference tables in the *Hom* scenario. This allows to compute BER thanks to the classical expressions of the BER of M-ary QAM constellations [31]. As expected, the obtained BER performance confirms the EVM behaviour is presented in Figure 7, and again, the PSD-based model is totally wrong for modelling the interference seen by the incumbent $\mathcal{U}_1$ in the *Het* scenario. Nevertheless, it gives a satisfying approximation of the BER of OFDM/OQAM based $\mathcal{U}_2$, especially for values of BER higher than 10^{-3}. However, when the BER of OFDM/OQAM based $\mathcal{U}_2$ becomes low (for $\sigma^2_{d_2} > 10$ dB), the PSD-based model underestimates it.

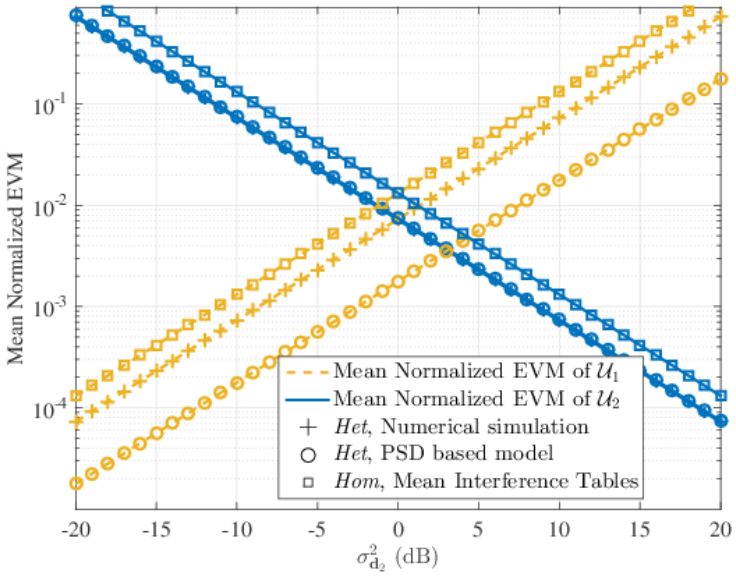

Figure 7: Mean Normalized EVM of users $\mathcal{U}_1$ and $\mathcal{U}_2$ in the scenarios *Het* and *Hom*

Finally, Figure 8 shows that the benefits of using OFDM/OQAM are not as high as what was expected with the PSD-based model. Yet, it shows that using OFDM/OQAM for the secondary $\mathcal{U}_2$ does still bring some advantage. For example, when both users have the same transmission power, the BER of each user in the *Het* scenario is equal to half what they experience in the *Hom* scenario.
Presented results show that, in scenarios where an incumbent CP-OFDM system coexists with an asynchronous user $\mathcal{U}_2$, it is still advantageous to both users that $\mathcal{U}_2$ uses OFDM/OQAM, though benefits are much less important than those planned with the PSD-based model in [26], [27]. To conclude this study, we focus on the BER of the incumbent $\mathcal{U}_1$ in both *Het* and *Hom* scenarios with a deterministic value of τ.

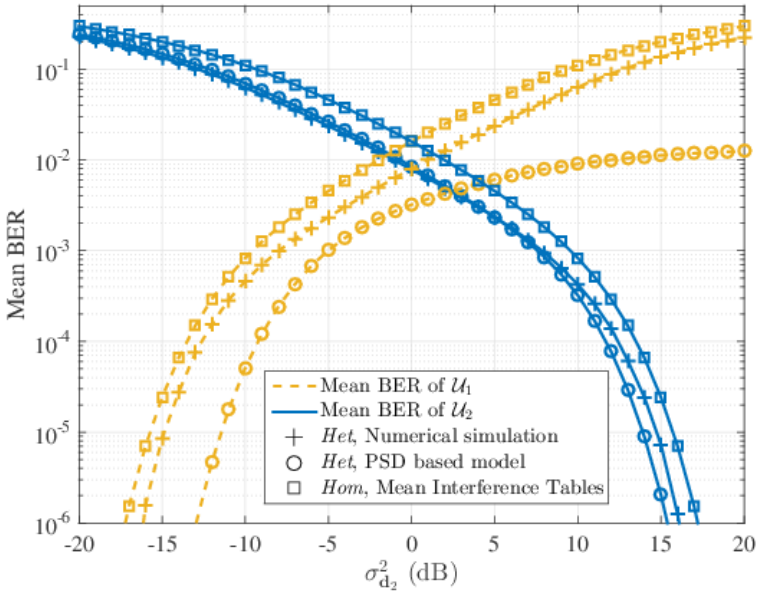

Figure 8: Mean BER of users $\mathcal{U}_1$ and $\mathcal{U}_2$ in the scenarios *Het* and *Hom*

3.5 Main conclusions

In this Section 3, we investigated a scenario where a D2D pair coexists with an OFDM based incumbent network. The D2D pair is allowed to use an alternative 5G waveform to OFDM. Time-frequency misalignment of the D2D was taken into account to generate the interference tables from different waveforms to an OFDM receiver. This is in contrast to the usual trend in sensitivity analysis available in the literature where the same waveform is considered for the source and the victim of interference. Through numerical results, we have shown that it is not worth synchronizing the D2D pair in time domain with respect to the incumbent network. Interference tables provided in this Section 3 allowed us to analyse the maximum rate achievable by the D2D pair under different interference constraints. We have shown that the communication window size has a direct impact on the efficacy of the waveform utilized by the D2D pair. For short D2D transmission windows, OFDM, GFDM and Lapped FBMC seem to be appropriate candidates. We also showed that under stringent interference constraints and wide transmission windows, OFDM/OQAM is strong candidates.

We showed that the widely used PSD-based model is highly flawed and fails to give a good approximation of the interference seen by each user in heterogeneous scenarios. Indeed, presented numerical results showed that when the secondary system utilizes OFDM/OQAM, the actual values of interference are higher than those planned by the PSD based model by more than 50 dB. Furthermore, contrary to the widely spread idea that CP-OFDM interferes more onto OFDM/OQAM users than the opposite, we revealed that heterogeneous interference is symmetrical and that users interfere equally onto each other.

Though it was shown that both users experience a slight improvement when the secondary user uses OFDM/OQAM modulation, the gain was shown to be much more limited than what was expected with the PSD-based model. Therefore, existing models in the literature to rate interference in heterogeneous networks are not satisfying.

4 FFT-FBMC waveform proposal for asynchronous communications

FFT-FBMC was proposed in [32][33] to combat the FBMC intrinsic interference and enable some MIMO techniques such as Space-time Blokc Coding (STBC) and Maximum-Likelihood Spatial Multiplexing (ML-SM). Indeed, FFT-FBMC performs FFT/IFFT precoding and postcoding on each subcarrier in order to get rid of the FBMC intrinsic interference. Not only does FFT-FBMC allow the straightforward application of MIMO techniques such as STBC and ML-SM, but also we will show that the signal is better localized in frequency domain [34]. However, one may wonder if the FBMC robustness against time misalignment in asynchronous contexts is still preserved with the FFT-FBMC scheme. Indeed, the timing asynchronism between coexisting systems can harmfully affect the performance by causing the asynchronous interference. Moreover, in some

cases (cognitive radio, Device-to-Device communications, non cooperative base stations,...), it is either costly or not possible to synchronize the different transmitters and receivers. Consequently, it is also relevant to evaluate the impact of this asynchronism on the FFT-FBMC performance.

4.1 Principle of FFT-FBMC waveform

Before being fed to the FBMC modulator, the data symbols in each subcarrier are first precoded. Consider a system with M subcarriers. On each subcarrier $k \in \{0, \ldots, M-1\}$, the QAM symbols $d_{k,n}$ are aggregated into groups of $\frac{N}{2} \in N^*$ symbols. Each group of N/2 symbols goes through a N-IFFT operation whose outputs $a_{k,n}$ are optionally extended with a cyclic prefix (CP) of size L [32]. The complex symbols $a_{k,n}$ on each subcarrier k can be written as [32]:

$$a_{k,n} = \frac{e^{j\pi n(k+1)}}{\sqrt{N}} \sum_{l=0}^{\frac{N}{2}-1} d_{k,l,p} e^{j2\pi \frac{nl}{N}}, \qquad \forall n \in B_p \tag{4.1-1}$$

where B_p represents the index set of symbols $a_{k,n}$ that belong to the p-th block of length N+L and is given by

$$B_p = \{(p-1)(N+L), \ldots, p(N+L)-1\}$$

and $d_{k,l,p}$ denotes the data $d_{k,l}$ transmitted in the p-th block of length N. After that, the precoded complex symbols $a_{k,n}$ are fed to the FBMC modulator whose output is given by [10]:

$$s[m] = \sum_{k=0}^{M-1} \sum_{n=-\infty}^{+\infty} a_{k,n} \underbrace{g[m - M/2] e^{j\frac{2\pi k}{M}(m-D)} e^{j\varphi_{k,n}}}_{g_{k,n}[m]} \tag{4.1-2}$$

where $g[m]$ is a prototype filter with length of $L_g = KM$ with $K \in N^*$ is called the overlapping factor, D is a delay term given by $D = (L_g - 1)/2$ to insure the causality of the prototype filter [10], and $\varphi_{k,n}$ is a phase term which can be given by $\varphi_{k,n} = \frac{\pi}{2}(n+k) - \pi kn$ [10]. The term $g_{k,n}[m]$ is defined as the frequency-time shifted version of $g[m]$.

At the receiver side, the FBMC demodulation is applied to recover the precoded symbols $\tilde{a}_{k,n}$which can be written as:

$$\tilde{a}_{k,n} = h_k \sum_{m=-\infty}^{+\infty} \sum_{k\prime=0}^{M-1} \sum_{n\prime \in Z} a_{k\prime,n\prime} g_{k\prime,n\prime}[m] g_{k,n}^*[m] + b_{k,n} \tag{4.1-3}$$

where h_k is the channel coefficient at subcarrier k and $b_{k,n}$ is the noise term at the frequency-time position (k,n). After that, the demodulated QAM data symbols $\tilde{d}_{k,l,p}$ $(\forall l \in \{0, \ldots, N/2\},\ \forall p \in Z)$ are obtained by:

$$\tilde{d}_{k,l,p} = \frac{h_k^{-1}}{\sqrt{N}} \sum_{n=(p-1)(N+L)}^{p(N+l)-L-1} \tilde{a}_{k,n} e^{j\pi n(k+1)} e^{-j2\pi \frac{nl}{N}} \tag{4.1-4}$$

4.2 PSD analysis

Let us consider that only one subcarrier k is activated. Therefore according to (4.1-2), the transmitted signal $s_k[m]$ can be given by:

$$s_k[m] = \frac{1}{\sigma_s} e^{j\frac{2\pi k}{M}(m-D)} \sum_{n=-\infty}^{+\infty} \underbrace{a_{k,n} e^{j\phi_{k,n}}}_{b_{k,n}} g[m - nM/2]$$

(4.2-1)

The Power Spectral Density (PSD) of the signal $s[m]$, disregarding the frequency shift term $e^{j\frac{2\pi k}{M}(m-D)}$, is given by [35]:

$$S(f) = \frac{2}{\sigma_s^2} |G(f)|^2 A\left(\frac{M}{2} f\right),$$

(4.2-2)

where $A\left(\nu = \frac{M}{2} f\right)$ is the PSD of $b_{k,n}$, $G(f)$ is the Fourier transform of the prototype filter $g[m]$, and f is the normalized frequency with respect to the sampling frequency f_s. Since $b_{k,n}$ is a discrete random process, its PSD is derived by calculating the Fourier transform of its autocorrelation function $\mathbb{E}\{b_{k,n} b_{k,n'}^*\}$. According to the definition of $b_{k,n}$ in (4.2-1), we have

$$\mathbb{E}\{b_{k,n} b_{k,n'}^*\} = \mathbb{E}\{a_{k,n} a_{k,n'}^*\} e^{j\phi_{k,n} - j\phi_{k,n'}}$$

(4.2-3)

Then, let us determine the analytic expression of $\mathbb{E}\{a_{k,n} a_{k,n'}^*\}$. Making use of (4.1-1),

$$\mathbb{E}\{a_{k,n} a_{k,n'}^*\} = \frac{1}{N} \sum_{l=0}^{\frac{N}{2}-1} \sum_{l'=0}^{\frac{N}{2}-1} \mathbb{E}\left\{d_{k,l,p} d_{k,l',p'}^*\right\} e^{j\frac{2\pi(nl - n'l')}{N}} e^{j\pi(k+1)\delta n}, \quad (n, n') \in B_p \times B_{p'},$$

(4.2-4)

where $\delta n = n - n'$. Since the data symbols $d_{k,l,p}$ are assumed to be statistically independent, we have

$$\mathbb{E}\left\{d_{k,l,p} d_{k,l',p'}^*\right\} = \sigma_d^2 \delta[l - l'] \delta[p - p'],$$

(4.2-5)

where $\delta[.]$ stands for the Kronecker function. Therefore,

$$\mathbb{E}\{a_{k,n} a_{k,n'}^*\} = \begin{cases} \frac{\sigma_d^2}{N} \sum_{l=0}^{\frac{N}{2}-1} e^{j\frac{2\pi l \delta n}{N}} e^{j\pi(k+1)\delta n}, & (n, n') \in B_p^2 \\ 0, & \text{elsewhere} \end{cases}$$

(4.2-6)

and then according to (4.2-3), we have

$$\mathbb{E}\{b_{k,n} b_{k,n-\delta n}^*\} = \mathbb{E}\{a_{k,n} a_{k,n-\delta n}^*\} e^{j\phi_{k,n} - j\phi_{k,n-\delta n}}$$
$$= \begin{cases} \frac{\sigma_d^2}{N} \sum_{l=0}^{\frac{N}{2}-1} e^{j\frac{2\pi l \delta n}{N}} e^{j\frac{3\pi}{2}\delta n} & (n, n - \delta n) \in B_p^2 \\ 0 & \text{Otherwise} \end{cases}$$

(4.2-7)

We recall that $B_p = \{(p-1)(N+L), \ldots, p(N+L) - 1\}$, with $p \in \mathbb{Z}$ ($\mathbb{Z}$ being the set of integer numbers). Therefore, $b_{k,n}$ is a non-stationary process as its autocorrelation function still depends on the time index "n". Therefore, we define the time-varying spectrum of $b_{k,n}$ as [36]:

$$A_n(\nu) = \sum_{\delta n=-\infty}^{+\infty} \mathbb{E}\{b_{k,n} b_{k,n-\delta n}^*\} e^{-j2\pi\nu\delta n}.$$

(4.2-8)

According to the expression of $\mathbb{E}\{b_{k,n} b_{k,n-\delta n}^*\}$ in (4.2-7), we can write, for $n \in B_p$:

$$\begin{aligned} A_n(\nu) &= \sum_{\delta n=n+1-p(N+L)}^{n-(p-1)(N+L)} \frac{\sigma_d^2}{N} \sum_{l=0}^{\frac{N}{2}-1} e^{j\frac{2\pi l\delta n}{N}} e^{j\frac{3\pi}{2}\delta n} e^{-j2\pi\nu\delta n} \\ &= \frac{\sigma_d^2}{N} \sum_{l=0}^{\frac{N}{2}-1} \sum_{\delta n=n+1-p(N+L)}^{n-(p-1)(N+L)} e^{j\left(\frac{2\pi l}{N}+\frac{3\pi}{2}-2\pi\nu\right)\delta n} \end{aligned},$$

(4.2-9)

We can easily show that $A_n(\nu)$ is periodic with respect to n with a period of $N + L$. Hence, the PSD $A(\nu)$ is calculated by averaging $A_n(\nu)$ with respect to n over one single period [36]:

$$A(\nu) = \frac{1}{N+L} \sum_{n\in B_1} A_n(\nu) = \frac{1}{N+L} \sum_{n=0}^{N+L-1} A_n(\nu).$$

(4.2-10)

For the sake of writing simplicity, let us set $X_l(\nu) = \frac{2\pi l}{N} + \frac{3\pi}{2} - 2\pi\nu$. We have:

$$\sum_{\delta n=n+1-p(N+L)}^{n-(p-1)(N+L)} e^{jX_l(\nu)\delta n} = \begin{cases} \dfrac{1-e^{jX_l(\nu)(N+L)}}{1-e^{jX_l(\nu)}} e^{jX_l(\nu)\left(n+1-p(N+L)\right)} & \dfrac{X_l(\nu)}{2\pi} \notin \mathbb{Z} \\ N+L & \dfrac{X_l(\nu)}{2\pi} \in \mathbb{Z} \end{cases}$$

(4.2-11)

Therefore, we can distinguish two cases for the expressions of $A_n(\nu)$ and $A(\nu)$ according to the frequency values ν:

- $\frac{X_l(\nu)}{2\pi} \notin \mathbb{Z}$, $\forall l \in \{0, \ldots, \frac{N}{2} - 1\}$: in this case, equation (4.2-9) is expressed as

$$A_n(\nu) = \frac{\sigma_d^2}{N} \sum_{l=0}^{\frac{N}{2}-1} \frac{1-e^{jX_l(\nu)(N+L)}}{1-e^{jX_l(\nu)}} e^{jX_l(\nu)(n+1-p(N+L))},$$

(4.2-12)

and then, (4.2-10) becomes

$$A(\nu) = \frac{\sigma_d^2}{N(N+L)} \sum_{l=0}^{\frac{N}{2}-1} \frac{1-e^{jX_l(\nu)(N+L)}}{1-e^{jX_l(\nu)}} \sum_{n=0}^{N+L-1} e^{jX_l(\nu)(n+1-N-L)}$$
$$= \frac{\sigma_d^2}{N(N+L)} \sum_{l=0}^{\frac{N}{2}-1} \frac{\sin\left(\frac{X_l(\nu)(N+L)}{2}\right)^2}{\sin\left(\frac{X_l(\nu)}{2}\right)^2}.$$

(4.2-13)

• $\exists l' \in \{0,\dots,\frac{N}{2}-1\}, \frac{X_{l'}(\nu)}{2\pi} \in \mathbb{Z}$: this second case yields that

$$l' = (\nu - \frac{3}{4} + q)N \quad q \in \mathbb{Z}.$$

As $l' \in \{0,\dots,\frac{N}{2}-1\}$, then there is at most one single pair (l', q) that satisfies the above condition for a given value of ν. Therefore, without loss of generality, we can restrict the condition above as

$$l' = N\left|\nu - \frac{3}{4}\right|_1.$$

where $|x|_p$ stands for the modulo operation of x by p. Hence, in this case, equation (4.2-9) is expressed as

$$A_n(\nu) = \frac{(N+L)\sigma_d^2}{N} + \frac{\sigma_d^2}{N} \sum_{\substack{l=0 \\ l \neq N\left|\nu-\frac{3}{4}\right|_1}}^{\frac{N}{2}-1} \frac{1-e^{jX_l(\nu)(N+L)}}{1-e^{jX_l(\nu)}} e^{jX_l(\nu)(n+1-p(N+L))}.$$

(4.2-14)

Then, (4.2-10) becomes :

$$A(\nu) = \frac{(N+L)\sigma_d^2}{N} + \frac{\sigma_d^2}{N(N+L)} \sum_{l=0 \; l \neq N\left|\nu-\frac{3}{4}\right|_1}^{\frac{N}{2}-1} \frac{\sin\left(\frac{X_l(\nu)(N+L)}{2}\right)^2}{\sin\left(\frac{X_l(\nu)}{2}\right)^2}.$$

(4.2-15)

Therefore, according to the values of ν, the PSD of $b_{k,n}$ is given by either (4.2-13) or (4.2-15). In order to gather the two expressions of the PSD of $b_{k,n}$ in a single expression, let us define $\mathbb{G}$ as the set of ν where the condition of the second case is satisfied. That is, $\mathbb{G} = \left\{\nu \;\middle|\; N\left|\nu - \frac{3}{4}\right|_1 \in \{0,\dots,\frac{N}{2}-1\}\right\}$. Thus, we can rewrite the expression of $A(\nu)$ as:

$$A(\nu) = \frac{(N+L)\sigma_d^2}{N} 1_{\{\nu\in\mathbb{G}\}} + \frac{\sigma_d^2}{N(N+L)} \sum_{l=0 \; l \neq N\left|\nu-\frac{3}{4}\right|_1}^{\frac{N}{2}-1} \frac{\sin\left(\frac{X_l(\nu)(N+L)}{2}\right)^2}{\sin\left(\frac{X_l(\nu)}{2}\right)^2},$$

(4.2-16)

where $1_{\{.\}}$ is the indicator function. According to the expression above, we can remark that $A(\nu)$ is periodic with a period of 1, which fits well with the sampling theory. Figure 9 depicts the curve of $A(\nu)$ for two different parameters: $(N, L) = (16,0)$ and $(N, L) = (64,2)$.

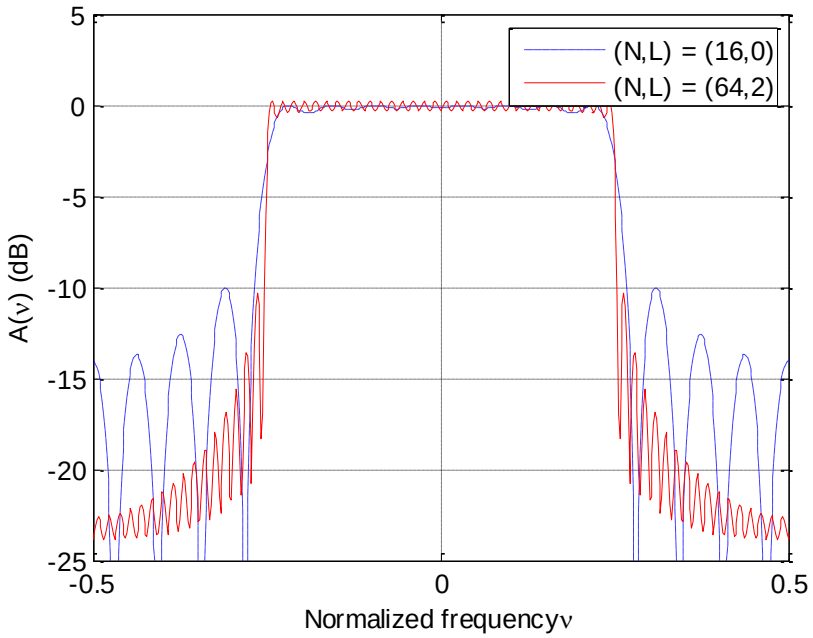

Figure 9: PSD curve $A(\nu)$ with two different parameters: $(N, L) = (16,0)$ and $(N, L) = (64,2)$.

Finally, the PSD of FFT-FBMC transmitted signal is obtained according to (4.2-2), where $|G(f)|^2$ is the PSD of the prototype filter. According to (4.2-16), $A(\nu)$ is a sum of $N/2$ shifted $\frac{\sin((N+L)x)^2}{\sin(x)^2}$ functions. It is worth noting that for a larger $(N + L)$, the main lobe of these shifted functions gets more concentrated. As a consequence, the PSD $S(f)$ of the transmitted signal are more confined in the considered band when $(N + L)$ is large.

When large number of subcarriers are activated, the PSD of the transmitted signal is the summation of the PSD of the signals in each activated subcarrier. For instance, Figure 10 depicts the PSD of FBMC and FFT-FBMC with one activated resource block (RB) of 12 subcarriers, where PHYDYAS filter [23] with overlapping factor of 4 is used. In general, any prototype filter can be considered. However, we chose PHYDYAS filter for its rapid-decaying property.

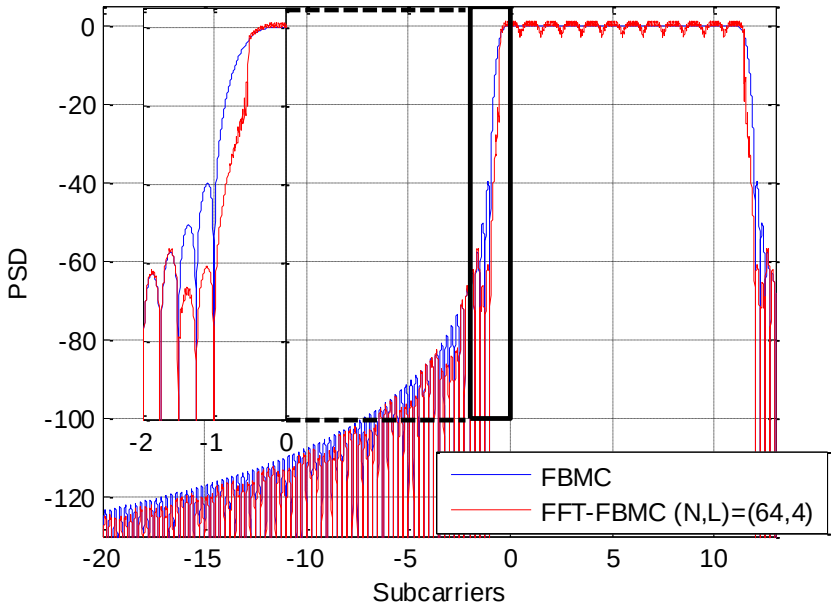

Figure 10: PSD comparison between FBMC and FFT-FBMC ($N = 64, L = 4$) signals using PHYDYAS filter with one activated RB.

The curves show that the spectral leakage in FFT-FBMC is lower than in FBMC. We especially would like to emphasize that the spectral leakage in the first adjacent subcarrier is significantly reduced in FFT-FBMC. This may allow, for example, asynchronous multi-user access without any guard band. Indeed, we consider in FBMC/PHYDYAS that a given subcarrier interferes only with the two direct adjacent ones. Whereas in FFT-FBMC the interference in immediate adjacent subbands is considerably reduced. We also depict in Figure 11 the PSD of two adjacent activated resource blocks for FBMC and FFT-FBMC. Clearly, the impact of inter-resource-block interferences is less severe in FFT-FBMC than in FBMC case.

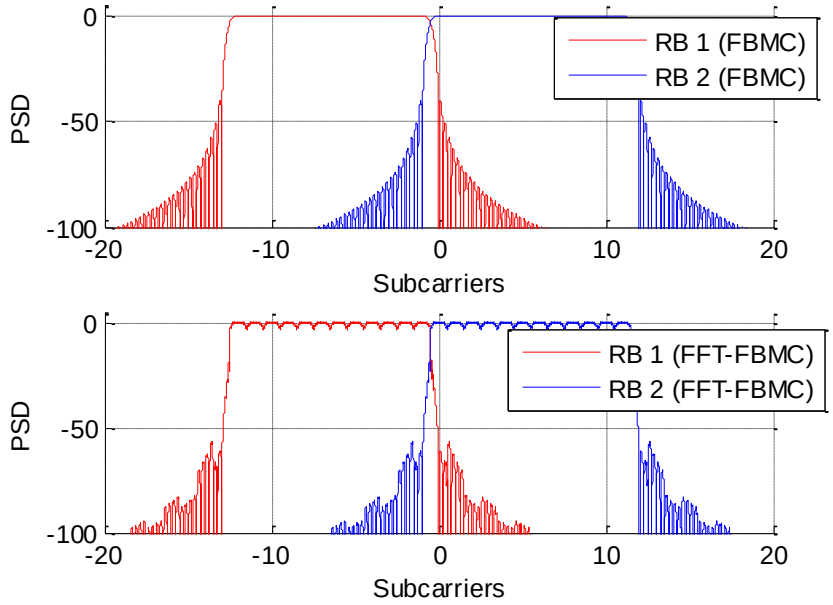

Figure 11: PSD curves of FBMC and FFT-FBMC for two adjacent RBs.

We also validate the obtained results by numerical simulations. We consider multicarrier modulation FBMC and FFT-FBMC with $M = 512$ subcarriers that only one of them is activated. For FFT-FBMC, we consider $N = 64$ and $L = 4$. In Figure 12, we compare the theoretical curve of $A(v)$ function (obtained by (4.2-16)) with the one obtained by simulation. We also compare the theoretical and simulation curves of the FFT-FBMC PSD in Figure 13. The simulation curves are obtained by averaging the PSD over 1000 realizations. Both figures clearly show that the theoretical curves fit well with the simulation ones.

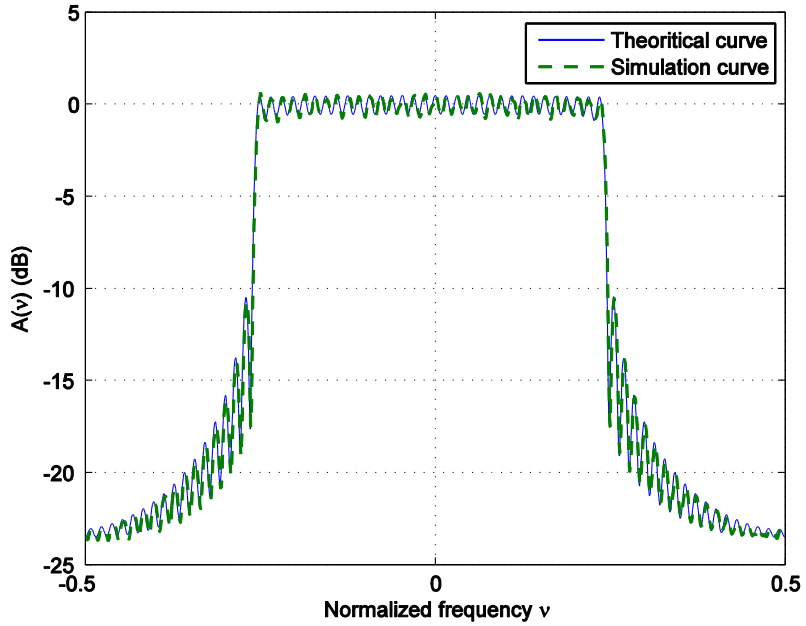

Figure 12: Comparison between theoretical and simulation PSD curve, $A(\nu)$ with $N = 64$ and $L = 4$.

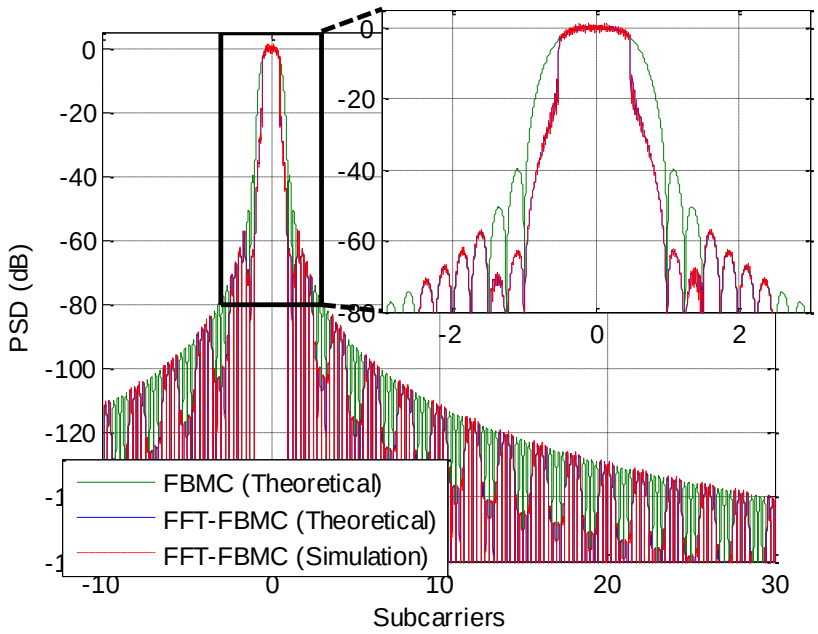

Figure 13: Comparison between theoretical and simulation curves of the PSD of FFT-FBMC

We have also numerically evaluated the signal energy spread over the activated subband and the three adjacent ones. Table 3 depicts, in terms of percentage and dB, the ratio of the energy signal in a given subband k to the whole transmitted signal energy for both FBMC and FFT-FBMC. It is assumed that the signal is only transmitted in subband $k = 0$. Then, we obtained about 98.74% of the whole FFT-FBMC transmitted energy in the subband $k = 0$. Whereas, in FBMC, 87.38% of the whole signal energy is in the activated subband. Therefore, FFT-FBMC leads to a lower spectrum leakage.

Table 3: Repartition of transmitted signal energy

	FFT-FBMC		FBMC	
$k = 0$	98.74 %	$-0.055\ dB$	87.38 %	$-0.585\ dB$
$k = 1$	0.16 %	$-27.87\ dB$	6.21%	$-12.07\ dB$
$k = 2$	3.58e-5 %	$-64.46\ dB$	3.14e-5%	$-65.02\ dB$

We also observe that FFT-FBMC reduces the interference power in the first adjacent subband of about 15.8 dB.

4.3 Interference analysis in asynchronous communications

In this section, we consider two asynchronous Device-to-Device (D2D) pairs (a) and (b) that coexist in the same geographical area. We assume that both D2D pairs share a given frequency band where B_a and B_b are the frequency subbands occupied by D2D pairs (a) and (b), respectively. Due to the timing offset between the D2D pairs, some amount of the power is spilled from a D2D pair to the other.
To evaluate the interference caused by the imperfect synchronization in FFT-FBMC, we consider the system model proposed in [30]. We focus on one receiver which suffers from the interference coming from the unsynchronized transmitter. This receiver is assumed to be perfectly synchronized with its corresponding transmitter. We assume that the interferer transmitter utilizes only one subcarrier q to transmit its signal. We therefore evaluate the instantaneous interference power $I_k^q[\tau]$ injected to the kth subcarrier of the victim D2D receiver by the interferer signal. We point out that when a larger number of subcarriers are utilized by the D2D pair, the total interference is equal to the sum of the interference caused by each subcarrier.

As the FFT-FBMC signal is processed in block-wise manner of size $NM/2$, the instantaneous interference $I_k^q[\tau]$ is evaluated for each timing offset τ which is assumed to be in the set $\{-NM/4, \dots, NM/4 - 1\}$ [37]. Since the timing offset τ is a random variable, it is also worth considering the average interference. However, there is a question that can be raised regarding the set of τ with respect to which the interference should be averaged. Hence, we have proposed to consider two contexts. The first one is to assume that the D2D pairs are totally unsynchronized and thus τ is uniformly distributed in the set $\{-NM/4, \dots, NM/4 - 1\}$ [37]. Therefore, the mean interference is calculated by averaging the interference $I_k^q[\tau]$ over the whole block of size $NM/2$ samples:

$$I_1[|k-q|] = \frac{2}{NM} \sum_{\tau=-MN/4}^{MN/4-1} I_k^q[\tau].$$

(4.3-1)

he second context is to assume that the D2D pairs are somehow or other grossly synchronized where the offset timing can be considered uniformly distributed on one multicarrier symbol duration (M), *i.e.* $\tau \in \{-M/2, \dots, M/2 - 1\}$ [37]. Therefore, the mean interference is calculated by averaging the interference $I_k^q[\tau]$ over one multicarrier symbol duration:

$$I_2[|k-q|] = \frac{1}{M} \sum_{\tau=-M/2}^{M/2-1} I_k^q[\tau].$$

4.3-2)

The total mean interference seen by the receiver (a) in the band (B_a) from the interferer (b) transmitting in the band (B_b) is the double sum of the contribution of each interfering subcarrier $q \in B_b$ on each subcarrier $k \in B_a$ [28]:

$$I_i(B_a, B_b) = \sum_{k \in B_a} \sum_{m \in B_b} I_i[|k-q|] P_q$$

(4.3-3)

where P_q is the interferer transmitted power in the qth subcarrier, and $i \in \{1,2\}$ is an index selecting the context case ($I_1(B_a, B_b)$ or $I_2(B_a, B_b)$).

We compute the interference seen by a D2D receiver in the lth subcarrier caused by an unsynchronized D2D interferer transmitting on a subcarrier $q = 0$. As previously mentioned, the interference $I_k^0[\tau]$ is calculated by simulation for each timing offset $\tau \in \{-NM/4, \ldots, NM/4 - 1\}$. We have considered the FFT-FBMC systems with $M = 512$ subcarriers and different pairs of the parameters $(N, L) \in \{16,32,64\} \times \{0,2,4\}$. The interferences that are injected by the interferer subcarrier $q = 0$ with unitary power on 10 neighboring subcarriers as a function of τ are depicted in Figure 14, Figure 15 and Figure 16 for different values of N and L.

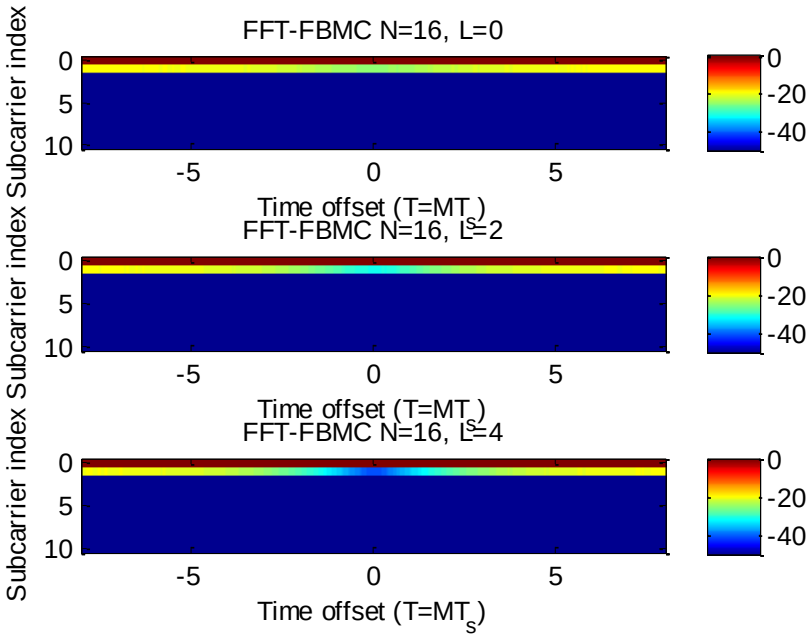

Figure 14: Interference in dB caused by an interferer D2D at subcarrier 0 on 10 neighboring subcarriers in function of τ for FFT-FBMC with $N = 16$.

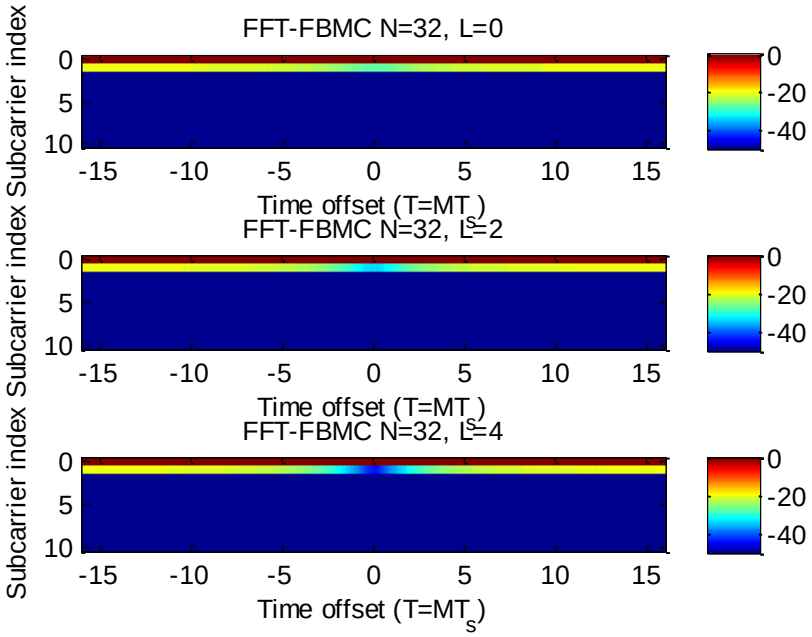

Figure 15: Interference in dB caused by an interferer D2D at subcarrier 0 on 10 neighboring subcarriers in function of τ for FFT-FBMC with $N = 32$.

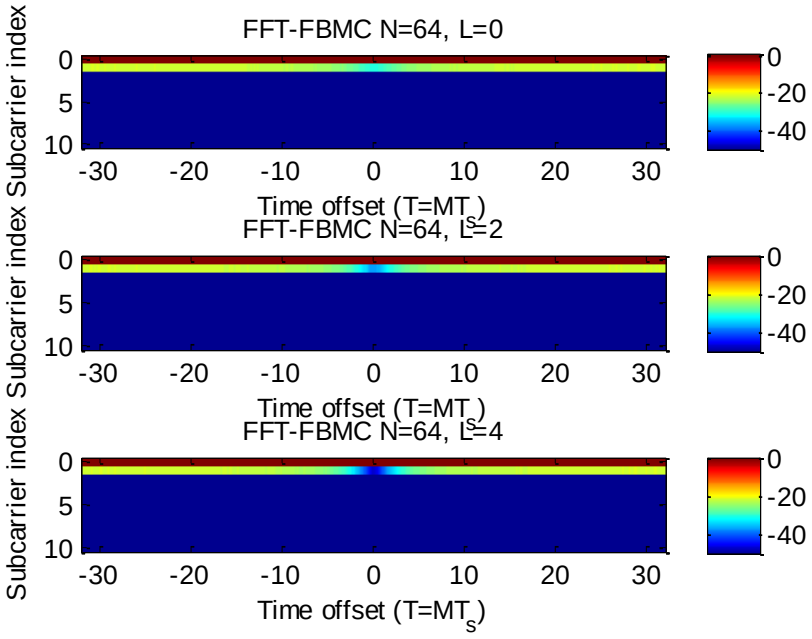

Figure 16: Interference in dB caused by an interferer D2D at subcarrier 0 on 10 neighboring subcarriers in function of τ for FFT-FBMC with $N = 64$.

One can observe that only the first adjacent subcarrier is affected by relatively high interference power. All the other subcarriers ($|k| > 1$) are subject to interference less than -50 dB. It is worth noticing that this feature is also present in FBMC waveform [28]. We also can remark that the interference level in the first adjacent subcarrier depends on the timing offset τ. In all configurations, the interference level reaches its maximum (around -20 dB) for the largest possible value of the timing offset ($|\tau| \to MN/2$). However, the lowest interference level, which is situated in the neighborhood of $\tau = 0$, depends on the parameters (N, L).

Figure 17, Figure 18 and Figure 19 depict the curves of the interference level of the first adjacent subcarrier ($k = 1$) as a function of the timing offset $\tau \in \{-MN/4, \ldots, MN/4 - 1\}$.

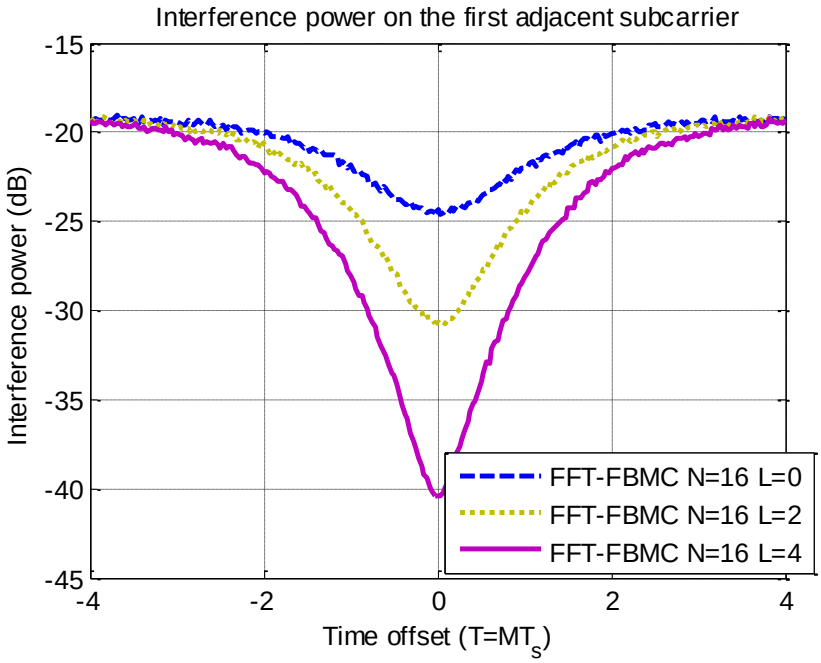

Figure 17: Interference level of the first adjacent subcarrier as a function of the timing offset for FFT-FBMC with $N = 16$.

The curves of the interference level for $N = 16$ and $L \in \{0,2,4\}$ are shown in Figure 17. We observe that the interference level for the different values of L and for $\tau = \pm 4$ is slightly higher than -20 dB. It is also shown that the interference value for $\tau = 0$ depends on the parameter L. When L is getting larger, the interference for $\tau = 0$ strongly decreases.

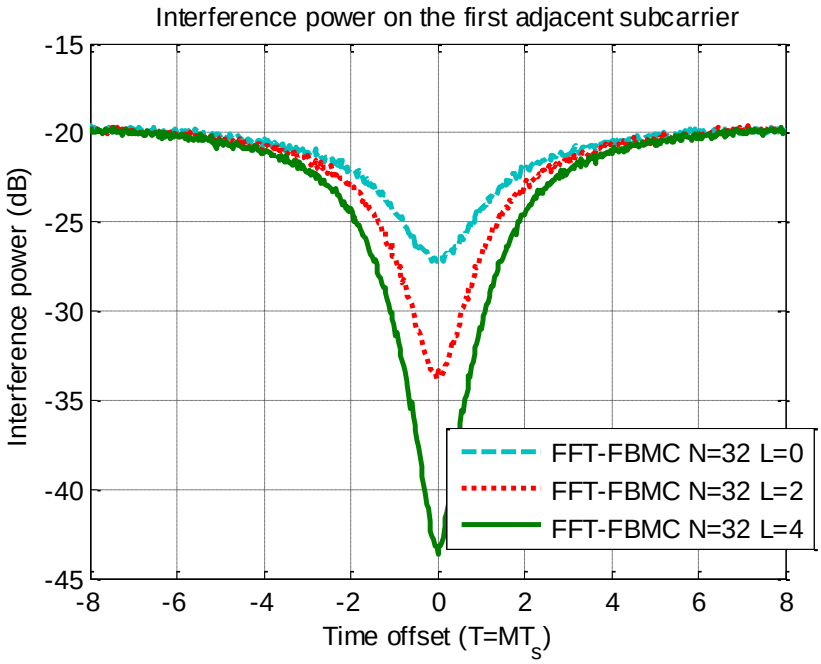

Figure 18: Interference level of the first adjacent subcarrier as a function of the timing offset for FFT-FBMC with $N = 32$.

Figure 18 depicts the curves of the interference level for $N = 32$ and $L \in \{0,2,4\}$. The same remarks as for $N = 16$ can be drawn for the case where $N = 32$. Moreover, by increasing N, we observe that interference levels for $\tau = 0$ are lower than in the previous figure ($N = 16$). For example, in Figure 18 for $(N, L) = (32,0)$

we have an interference for $\tau = 0$ of about -27 dB, whereas when $(N, L) = (16,0)$ the interference for $\tau = 0$ is about -24 dB (Figure 17).

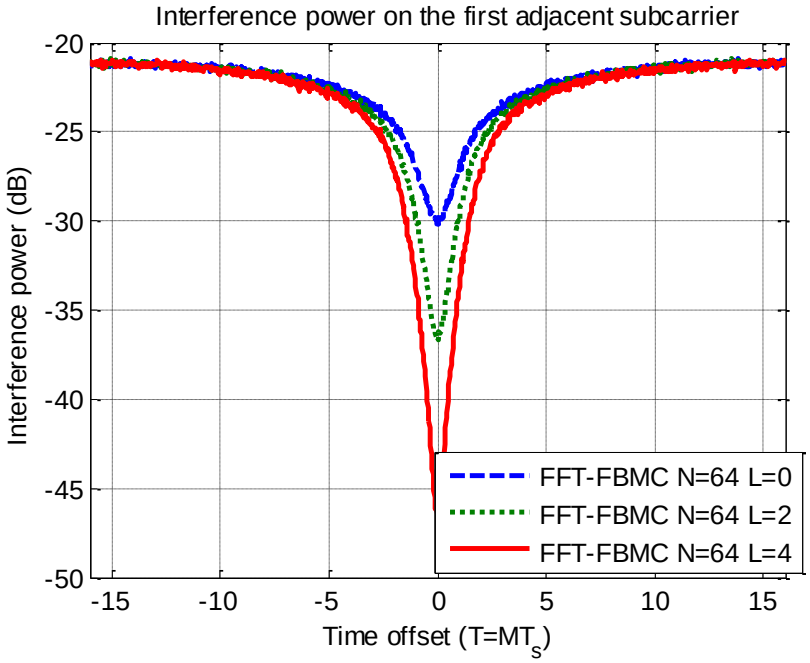

Figure 19: Interference level of the first adjacent subcarrier as a function of the timing offset for FFT-FBMC with $N = 64$.

As for the case where $N = 64$, Figure 19 shows that the interference levels for $\tau = 0$ fall even lower. For $L = 0$, we have an interference value (for $\tau = 0$) of -30 dB, whereas with the same value of $L = 0$ but with $N = 32$ and $N = 16$ the interference level is -27 dB and -24 dB, respectively.

According to these figures (Figure 17, Figure 18, and Figure 19), one can conclude that the interference level in the first adjacent subcarrier for large values of the timing offset τ does slightly change with respect to N and L. However, when $\tau = 0$ the interference level is strongly dependent on the values of N and L. Moreover, we can remark that the interference level for $\tau = 0$ does depend more on the L value than on N. Indeed, passing from $L = 0$ to $L = 2$ we obtain a gain of about 6 dB, and from $L = 2$ to $L = 4$ we gain 9 dB. Whereas, the interference is only reduced by 3 dB when passing from $N = 16$ to $N = 32$ or from $N = 32$ to $N = 64$.
As we have mentioned in the previous section, we can assume that the timing offset τ takes values within one multicarrier symbol duration ($\tau \in \{-M/2, \ldots, M/2 - 1\}$). In this case, we have depicted in Figure 20, Figure 21, and Figure 22, the curves of the interference level of the first adjacent subcarrier ($k = 1$) as a function of the timing offset $\tau \in \{-M/2, \ldots, M/2 - 1\}$.

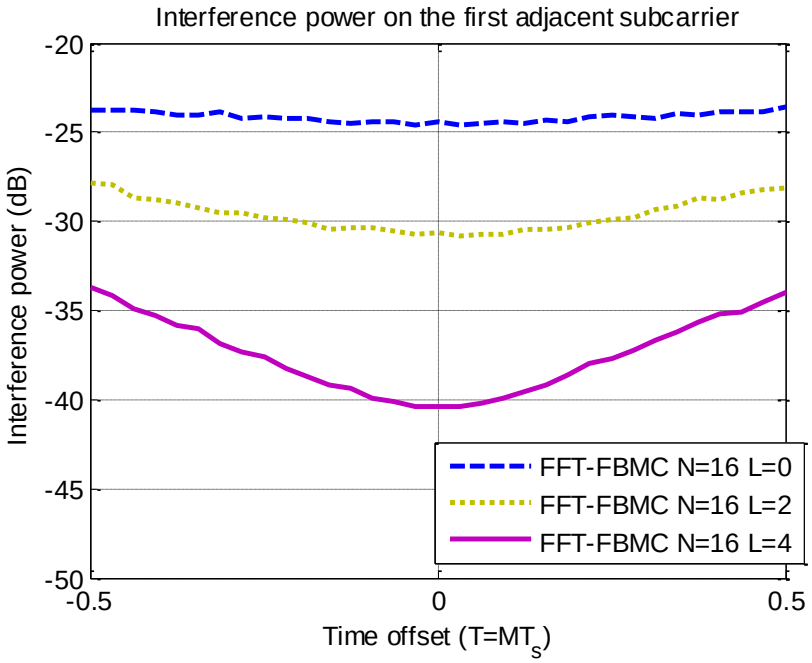

Figure 20: Interference level of the first adjacent subcarrier as a function of the timing offset $\tau \in \{-M/2, \ldots, M/2-1\}$ for FFT-FBMC with $N = 16$.

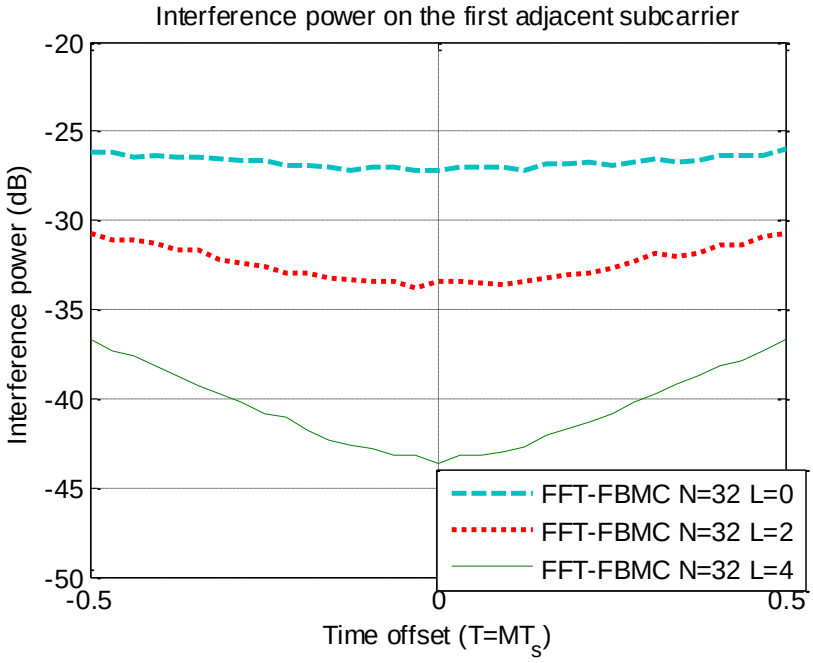

Figure 21: Interference level of the first adjacent subcarrier as a function of the timing offset $\tau \in \{-M/2, \ldots, M/2-1\}$ for FFT-FBMC with $N = 32$.

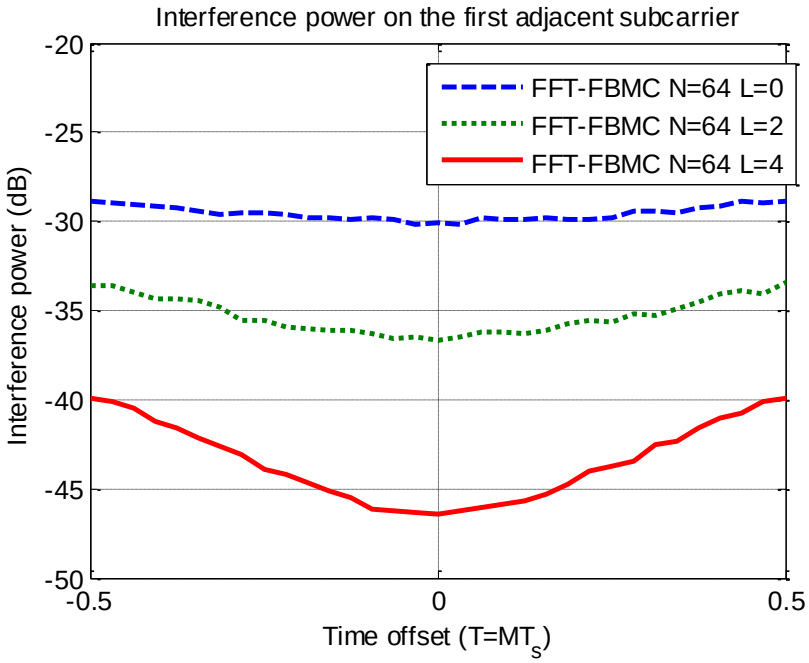

Figure 22: Interference level of the first adjacent subcarrier as a function of the timing offset $\tau \in \{-M/2, \ldots, M/2-1\}$ for FFT-FBMC with $N = 64$.

We remark that we can consider that the interference is almost invariant only when $L = 0$. We have a ratio between the interference level for $\tau = 0$ and $\tau = \pm M/2$ of about 1 dB.
Now, we consider the mean interference which is either averaged over the whole block of size $NM/2$ ($\tau \in \{-MN/4, \ldots, MN/4-1\}$) or averaged over one multicarrier symbol duration ($\tau \in \{-M/2, \ldots, M/2-1\}$). We compare the FFT-FBMC average interference for different configurations of (N, L) with that of FBMC [19]. The comparison of the interference values for the three subcarriers ($k = 0,1,2$) are depicted in Table 4 and Table 5. The interference levels are shown in both linear and decibel values.

The FFT-FBMC mean interference values averaged over the whole block are shown in Table 4. One can observe that for $k = 2$, the FFT-FBMC average interference is almost the same (about of -61 dB) for all the configurations of (N, L). Moreover, we have only a gain of less than 1 dB compared to FBMC (for $k = 2$). However, a significant interference reduction of FFT-FBMC compared to FBMC is observed for the first adjacent subcarrier $k = 1$. In FBMC, the first subcarrier is affected by an interference level of about -10.55 dB, whereas the interference for $k = 1$ is about -20.55 dB in the worst configuration of FFT-FBMC. Therefore, the mean interference level in the first adjacent subcarrier is at least reduced by 10 dB thanks to FFT-FBMC. This is explained by the spectrum leakage reduction shown in [34] for FFT-FBMC. Another observation could be drawn from Table 4 is that the mean interference level for $k = 1$ varies slowly with the configuration values of (N, L).

Table 4: Values of the interference power by averaging over the whole frame (NT/2)

			k=0	k=1	k=2
FFT-FBMC	N=16	L=0	0.9357	0.0088	7.25×10^{-7}
			-0.29 dB	-20.55 dB	-61.4 dB
		L=2	0.9448	0.0072	7.28×10^{-7}
			-0.24 dB	-21.38 dB	-61.38 dB
		L=4	0.9533	0.0058	7.3×10^{-7}
			-0.21 dB	-22.35 dB	-61.37 dB
	N=32	L=0	0.9588	0.0078	7.49×10^{-7}
			-0.18 dB	-21.06 dB	-61.25 dB
		L=2	0.9617	0.0072	7.51×10^{-7}
			-0.16 dB	-21.45 dB	-61.24 dB
		L=4	0.9647	0.0065	7.54×10^{-7}
			-0.16 dB	-21.87 dB	-61.23 dB
	N=64	L=0	0.9750	0.0060	7.69×10^{-7}
			-0.11 dB	-22.19 dB	-61.14 dB
		L=2	0.9759	0.0058	7.69×10^{-7}
			-0.11 dB	-22.37 dB	-61.14 dB
		L=4	0.9771	0.0055	7.70×10^{-7}
			-0.101 dB	-22.56 dB	-61.13 dB
FBMC			0.823	0.0881	1.11×10^{-6}
			-0.85 dB	-10.55 dB	-59.56 dB

Table 5: Values of the interference power by averaging over one symbol duration (T)

			k=0	k=1	k=2
FFT-FBMC	N=16	L=0	0.9588	0.0038	6.91×10^{-7}
			-0.18 dB	-24.14 dB	-61.6 dB
		L=2	0.9908	0.0011	6.8×10^{-7}
			-0.04 dB	-29.52 dB	-61.67 dB
		L=4	0.9980	0.0002	6.84×10^{-7}
			-0.009 dB	-36.94 dB	-61.65 dB
	N=32	L=0	0.9775	0.0021	7.38×10^{-7}
			-0.098 dB	-26.71 dB	-61.32 dB
		L=2	0.9949	0.0006	7.36×10^{-7}
			-0.02 dB	-32.31 dB	-61.33 dB
		L=4	0.9989	0.0001	7.42×10^{-7}
			-0.005 dB	-39.90 dB	-61.29 dB
	N=64	L=0	0.9889	0.0011	7.58×10^{-7}
			-0.048 dB	-29.53 dB	-61.21 dB
		L=2	0.9973	0.0003	7.58×10^{-7}
			-0.012 dB	-35.15 dB	-61.20 dB
		L=4	0.9994	5.16×10^{-6}	7.61×10^{-7}
			-0.003 dB	-42.87 dB	-61.19 dB
FBMC			0.823	0.0881	1.11×10^{-6}
			-0.85 dB	-10.55 dB	-59.56 dB

Table 5 shows that the average interference in subcarrier $k = 1$ strongly changes its values according to the parameters N and L. Compared to FBMC, we reduce the mean interference in subcarrier $k = 1$ by at least 14 dB.

4.4 Conclusion

In this Section, we have considered the FFT-FBMC system for asynchronous multi-user access. After a brief overview on the FFT-FBMC transmitter and receiver structure, we have derived the theoretical expression of the PSD of FFT-FBMC transmitted signal. We have shown that FFT-FBMC spectrum is better confined than the conventional FBMC one. By simulation, we have validated the developed expression of the FFT-FBMC, and evaluated the spectrum leakage to the adjacent subbands. We found that the interference power in the immediate adjacent subband is less in FFT-FBMC than in FBMC of about 15.8 dB.
After that, we have also analyzed the interference injected by an unsynchronized interferer transmitter into the adjacent subcarriers of a receiver when both of the interferer transmitter and receiver use the FFT-FBMC waveform. We have emphasized the fact that only the first adjacent subcarrier of the receiver is affected by a relatively high interference. Moreover, it has been shown that compared to FBMC the FFT-FBMC interference level in the immediate subcarrier is reduced by at least 10 dB. The low interference value in the first adjacent subcarrier in FFT-FBMC could allow the system to exploit this subcarrier for transmitting useful data, and avoid the insertion of guard subcarriers in subband edges.

5 General conclusions

Results provided from interference analysis using cited waveforms (in Section 2) shows that under stringent interference constraints and wide transmission windows, OFDM/OQAM (FBMC) is a strong candidate. Although we showed that the widely used PSD-based model is highly flawed and fails to give a good approximation of the interference seen by each user in heterogeneous scenarios, and by consequent the real injected interference in adjacent (in spectrum dimension) communications is much higher than predicted by the PSD model, we still experiment a gain in favour of the FBMC. This gain is becoming much more evident (see achieved results in Section 3 of D2.2) where it has been showed that the adoption of FBMC for D2D communication can indeed facilitate interference mitigation and therefore make the resource allocation procedures more efficient.

The proposed FFT-FBMC waveform provides an enhancement on the time-frequency localisation compared to the FBMC scheme. Significant interference reduction of FFT-FBMC compared to FBMC is observed for the first adjacent subcarrier $k = 1$ (following the PSD model). In FBMC, the first subcarrier is affected by an interference level of about -10.55 dB, whereas the interference for $k = 1$ is about -20.55 dB in the worst configuration of FFT-FBMC. Therefore, thanks to FFT-FBMC the mean interference level in the first adjacent subcarrier is at least reduced by 10 dB.

Further analysis will be carried out for a better understanding of the achieved coexistence capabilities of proposed FFT-FBMC and (classical) FBMC in D2D cellular context.

6 References

[1] 3GPP TR36.843, "Study on LTE device to device proximity services; Radio aspects (Release 12)," Tech. Rep., 2014.

[2] B. Aziz, I. Fijalkow, and M. Ariaudo, "Intercarrier interference in uplink OFDMA systems with carrier frequency offset," *21st Annual IEEE International Symposium on Personal, Indoor and Mobile Radio Communications*, pp. 746–751, Sep. 2010.

[3] A. Aminjavaheri, A. Farhang *et al.*, "Impact of Timing and Frequency Offsets on Multicarrier Waveform Candidates for 5G," 2015. http://arxiv.org/abs/1505.00800

[4] M. El-absi, M. Shaat *et al.*, "Power Loading and Spectral Efficiency Comparison of MIMO OFDM / BMC for Interference Alignment Based Cognitive Radio Systems," in *ISWCS*, 2014, pp. 480–485.

[5] Y. Ma, Y. Xu, and D. Zhang, "Power Allocation for Orthogonal Frequency Division Multiplexing-Based Cognitive Radio Systems with and without Integral Bit Rate Consideration," *IET Communications*, vol. 5, no. 5, p. 575, 2011.

[6] M. Shaat and F. Bader, "Low Complexity Power Loading Scheme in Cognitive Radio Networks: FBMC capability," in *IEEE International Symposium on Personal, Indoor and Mobile Radio Communications*, 2009, pp. 2597–2602.

[7] G. Bansal, J. Hossain, and V. K. Bhargava, "Adaptive Power Loading for OFDM-Based Cognitive Radio Systems," in *IEEE International Conference on Communications*, 2007, pp. 5137–5142.

[8] A. M. Tonello, "Performance Limits for Filtered Multitone Modulation in Fading Channels," *IEEE Transactions on Wireless Communications*, vol. 4, no. 5, pp. 2121–2135, 2005.

[9] M. Renfors, J. Yli-Kaakinen *et al.*, "ICT-Emphatic, D2.1: FB-MC and Enhanced OFDM Schemes," 2013.

[10] P. Siohan, C. Siclet, and N. Lacaille, "Analysis and design of OFDM/OQAM systems based on filterbank theory," *IEEE Transactions on Signal Processing*, vol. 50, no. 5, pp. 1170–1183, 2002.

[11] B. Farhang-Boroujeny, "OFDM versus filter bank multicarrier," *Signal Processing Magazine, IEEE*, no. MAY 2011, pp. 92–112, 2011.

[12] M. Bellanger, D. Mattera, and M. Tanda, "A Filter Bank Multicarrier Scheme Running at Symbol Rate for FutureWireless Systems," in *Wireless Telecommunications Symposium*, no. April, 2015.

[13] G. Fettweis, M. Krondorf, and S. Bittner, "GFDM-generalized frequency division multiplexing," in *IEEE Vehicular Technology Conference Spring*, 2009, pp. 1–4.

[14] N. Michailow, M. Matthe *et al.*, "Generalized Frequency Division Multiplexing for 5th Generation Cellular Networks," *IEEE Transactions on Communications*, vol. 62, no. 9, pp. 3045–3061, 2014.

[15] L. G. Baltar, D. S. Waldhauser, and J. A. Nossek, "Out-Of-Band Radiation in Multicarrier Systems: A Comparison," in *Multi-Carrier Spread Spectrum 2007*. Springer Netherlands, 2007, vol. 1, pp. 107–116.

[16] H. Mahmoud, T. Yucek, and H. Arslan, "OFDM for cognitive radio: merits and challenges," *IEEE Wireless Communications*, vol. 16, no. April, pp. 6–15, 2009.

[17] R. Chang, "High-speed multichannel data transmission with bandlimited orthogonal signals," *Bell Sys. Tech. J.*, vol. 45, pp. 1775–1796, Dec. 1966.

[18] A. Viholainen, M. Bellanger, and M. Huchard, "Prototype Filter and Structure Optimization," Phydias Project Consortium, Tech. Rep., 2009.

[19] Y. Medjahdi, M. Terré *et al.*, "Performance analysis in the downlink of asynchronous OFDM/FBMC based multi-cellular networks," *IEEE Transactions on Wireless Communications*, vol. 10, no. 8, pp. 2630–2639, 2011.

[20] K. Doppler *et al.*, "Device-to-Device Communication as an Underlay to LTE-Advanced Networks," *IEEE Commun. Mag.*, vol. 7, no. 12, 2009, pp. 42–49.

[21] J. Perez-Romero *et al.*, "A Novel On-Demand Cognitive Pilot Channel Enabling Dynamic Spectrum Allocation," *Proc. 2nd Int'l. Symp. New Frontiers in Dynamic Spectrum Access Networks*, Apr. 2007.

[22] Gábor Fodor, Erik Dahlman, Gunnar Mildh, Stefan Parkvall, Norbert Reider, György Miklós, and Zoltán Turányi, Ericsson Research, " Design Aspects of Network Assisted Device-to-Device Communications", IEEE Communications Magazine. pp. 170-177, March 2012

[23] M. Bellanger *et al.*, , "FBMC physical layer: a primer," pp. 1–31, 2010.

[24] H. Xing and M. Renfors, "Investigation of filter bank based device-to-device communication integrated into OFDMA cellular system," in *ISWCS*, 2014, pp. 513–518.

[25] R. Xu and M. Chen, “Spectral leakage suppression of DFT based OFDM via adjacent subcarriers correlative coding,” in *Proceedings of IEEE Global Telecommunications Conference (GLOBECOM ’08)*.pp. 3029–3033. December 2008.

[26] M. Shaat and F. Bader, “Computationally efficient power allocation algorithm in multicarrier-based cognitive radio networks: OFDM and FBMC systems,” *EURASIP Journal on Advances in Signal Processing*, vol. 2010, p. 5, 2010.

[27] A. Skrzypczak, J. Palicot, and P. Siohan, “OFDM/OQAM modulation for efficient dynamic spectrum access,” *International Journal of Communication Networks and Distributed Systems*, vol. 8, no. 3-4, pp. 247–266, 2012.

[28] Q. Bodinier *et al.*, “5G Waveforms for Overlay D2D Communications: Effects of Time-Frequency Misalignment,” in *IEEE International Conference on Communications (ICC)*, Kuala Lumpur, Malaysia 2016.

[29] A. K. T. Weiss, J. Hillenbrand and F. K. Jondral, “Mutual Interference in OFDM-Based Spectrum Pooling Systems,” in *Proceedings of the 59th IEEE Vehicular Technology Conference (VTC ’04). Milan, Italy*, vol. 59, 2004.

[30] Y. Medjahdi *et al.*, “Interference tables: a useful model for interference analysis in asynchronous multicarrier transmission,” *EURASIP Journal on Advances in Signal Processing*, vol. 2014, no. 54, pp. 1–17, 2014.

[31] J. G. Proakis, “Optimum Receivers for the Additive White Gaussian Noise Channel,” in *Digital Communications*, internatio ed., McGraw- Hill, Ed., 2001, pp. 231–332.

[32] R. Zakaria and D. Le Ruyet, "A Novel Filter-Bank Multicarrier Scheme to Mitigate the Intrinsic Interference: Application to MIMO Systems," in *IEEE Transactions on Wireless Communications*, vol. 11, no. 3, pp. 1112-1123, March 2012.

[33] R. Zakaria and D. Le Ruyet, "A novel FBMC scheme for Spatial Multiplexing with Maximum Likelihood detection," *2010 7th International Symposium on Wireless Communication Systems*, York, 2010, pp. 461-465.

[34] R. Zakaria and D. Le Ruyet, "Theoretical Analysis of the Power Spectral Density for FFT-FBMC Signals," in *IEEE Communications Letters*, vol. 20, no. 9, pp. 1748-1751, Sept. 2016.

[35] L.W. Couch. "Digital & Analog Communication Systems". *Prentice Hall*, 2012.

[36] W. A. Gardner, "Identification of systems with cyclostationary input and correlated input/output measurement noise," in *IEEE Transactions on Automatic Control*, vol. 35, no. 4, pp. 449-452, Apr 1990.

[37] R. Zakaria and D. Le Ruyet, "Interference analysis of FFT-FBMC scheme in time asynchronous contexts," *2016 International Symposium on Wireless Communication Systems (ISWCS)*, Poznan, 2016, pp. 225-229.

7 List of abbreviations

AC	Adaptive Clipping
AWGN	Additive White Gaussian Noise
BER	Bit Error Rate
CP	Cyclic Prefix
DFT	Discrete Fourier Transform
D2D	Device-to-Device
EVM	Error Vector Magnitude
FBMC	Filter Bank Multi-Carrier
FFT	Fast Fourier Transform
FMT	Filtered Multi-Tone modulation
GFDM	Generalized Frequency-Division Multiplexing
ICI	Inter-Carrier Interference
IDFT	Inverse Discrete Fourier Transform
LTE	Long Term Evolution
N-QAM	N Quadrature Amplitude Modulation
OFDM	Orthogonal frequency Division Multiple Access
OOB	Out Of Band
OQAM	Offset QAM
PAM	Pulse Amplitude Modulation
PSD	Power Spectral Density
QAM	Quadrature Amplitude Modulation
QPSK	Quadrature Phase Shift Keying
RC	Raised Cosine
RRC	Root Raised Cosine
RB	Resource Block
SC-FDMA	Single Carrier Frequency Division Multiple Access
TBW	Transition Bandwidth